RIVERBANK EROSION RATES

IN THE WHITE CLAY CREEK WATERSHED, PA

by

Kristen McCarthy

A thesis submitted to the Faculty of the University of Delaware in partial fulfillment of the requirements for the degree of Master of Science in Geology

Spring 2018

RIVERBANK EROSION RATES

IN THE WHITE CLAY CREEK WATERSHED, PA

by

Kristen McCarthy

Approved: ____
James E. Pizzuto, Ph.D.
Professor in charge of thesis on behalf of the Advisory Committee

Approved: ____
Neil Sturchio, Ph.D.
Chair of the Department of Geological Sciences

Approved: ____
Estella Atekwana, Ph.D.
Dean of the College of Earth, Ocean, and Environment

Approved: ____
Ann L. Ardis, Ph.D.
Senior Vice Provost for Graduate and Professional Education

ACKNOWLEDGMENTS

First and foremost, I would like to thank my advisor Dr. Jim Pizzuto for his guidance and support. I am incredibly grateful for the time he put aside to make sure I could succeed. I would like to thank thesis committee member Dr. Michael O'Neal for his advice and ability to always have the tool to fix the problem at hand. I would also like to thank thesis committee member Dr. Stephanie Stotts for her assistance with the process of analyzing tree roots and suggestions along the way.

This project could not have been completed without contributions from Elise Williamson (former University of Delaware master's student) for providing some quantified erosion rate data and Melinda Daniels (Stroud Water Research Center) for providing slope data for the sites located near SWRC.

I would also like to recognize a number of people for their fieldwork assistance, GIS help, and general advice, ideas, and encouragement. This includes Raphael Affinito for his countless number of hours spent in the field throughout the summer completed with a smile, despite the hot Delaware sun, Bill Parnella for his incredibly helpful problem solving ideas, Coty Cribb for his field help and patience in sharing his knowledge of GIS, Réjanne Le Bivic for her GIS preparatory work and advice, Vincent Onorato and Nick Tobia for their willingness to help in the field, and Tara Metzger, Olivia Gulledge, and Amanda Doremus for their incite related to analyzing tree roots. I also couldn't have done this without the encouragement and support of my office mate, Carlos Duque Calvache; friend, Coty Cribb; roommate, Gretchen Dykes; and my wonderful family.

TABLE OF CONTENTS

Appendix

LIST OF TABLES

LIST OF FIGURES

ABSTRACT

The supply of sediment to stream channels and estuaries is currently a concern in the Christina River basin. The goal of this study is to provide one component of the sediment budget for the White Clay Creek watershed, a primary watershed in the Christina basin, by quantifying the rates of stream bank erosion and factors that control bank erosion rates. At carefully chosen field sites, bank erosion rates have been estimated using historical aerial imagery and exposed tree root dendrochronology techniques. To explain variations in measured bank erosion rates, a variety of controls are considered including riparian vegetation, near-bank velocity, bank material strength, and the effects of freeze-thaw processes. Results show that for banks with a considerable number of riparian trees the bank erosion rates stay below 12.5 cm/yr, while banks with either no trees, smaller trees, or a small number of trees have erosion rates that vary from 9.9 cm/yr to 36.1 cm/yr. No correlation can be found between near-bank velocity or bank strength versus erosion rates, and the same applies for those sites not dominated by riparian trees. There seems to be some correlation between the material in the basal layer of the bank and bank erosion rates with an average bank erosion rate of 17.0 cm/yr for banks with a basal layer of mostly mud, and 9.5 cm/yr for banks with a basal layer of mostly sand and gravel. The results of this study will later be used to estimate bank erosion rates for the entire White Clay Creek watershed.

Chapter 1

INTRODUCTION

The supply of sediment to stream channels and estuaries is currently a concern in the Christina River basin, a watershed in the mid-Atlantic United States. According to the University of Delaware's Water Resources Agency, streams in the Delaware portion of the Christina River basin have impaired water quality in the form of high sediment loads. Management goals in the region include decreasing the sediment supply to the Christina River and ultimately the Delaware River and Bay (Kauffman, 2003). The Water Resources Agency reports that sediment loads from land and stream erosion sources total between 34.9 and 109.3 $t/km^2/yr$ in the Christina River basin, a value they hope to see decrease to less than 28.0 $t/km^2/yr$ (Kauffman, 2003).

Upland soil erosion, gully erosion, and stream banks have all been cited as sources of sediment to stream channels (Charlton, 2008). While gully erosion is often overlooked in management plans, local agencies have developed best management practices to minimize soil and bank erosion. In some counties within the watershed, design standards require a riparian buffer adjacent to streams and lakes, and many projects stress the role of riparian vegetation on slowing or preventing bank erosion (Code of Ordinances, 2016). One such management solution was conducted using "stunted log vanes" which slowed and stopped rapid bank erosion due to high flows along a tributary of the Christina River (accessed March 16, 2017 from http://duffnet.com/?page_id=521). Other projects in the Christina watershed have used large boulders to stabilize banks where erosion was harmful to aquatic habitats (accessed March 14, 2017 from https://www.epa.gov/ sites/production/files/ 2015-11/documents/ de_pikecreek.pdf). Once restoration projects are completed, it is important to understand the magnitude of potential benefits they create as well as how long it might take for benefits to reach downstream reaches.

Although there are popular methods to predict bank erosion, most are not reliable enough to be useful and many only apply to very specific reach conditions. Flaws in these methods include depending too much on channel form observations and classification of reaches, as well as assuming stable systems. Other methods make sweeping generalizations about the effects of grain size or depend too much on predictions of bankfull or effective discharge (Simon et al., 2007; Lawler, 1993; Evans et al., 2003; Rosgen, 2001). To find better ways to predict bank erosion rates, we must further understand the controls on bank erosion processes which, first and foremost, includes directly measuring erosion rates.

1.1 Bank Erosion Processes

High rates of bank erosion can result in loss of land, increased sedimentation in downstream areas, loss of riparian and floodplain structures, and increased inputs of legacy contaminants to waterways. With an increase in bank erosion compared to deposition, the stream's sediment load will increase (Charlton, 2008), potentially changing a river's planform (Smith and Smith, 1984) or other morphological variables. In a bedrock channel, additional bedload sediment from upstream can increase the number of sediment to bedrock impacts per unit time and area, causing abrasion and quarrying downstream (Turowski et al., 2008). Erosional processes that increase the amount of suspended sediment in a stream can influence water quality (Bricker et al., 1994; Perlman, 2014) and biogeochemical stream processes as well as smother habitat features required for many different types of organisms (Nimick et al., 2010). Decreases in erosion rates can also cause lasting changes to downstream reaches of a stream. This means that any sudden change to geomorphic processes can alter the ecosystem and surrounding landforms in a variety of ways.

Fortunately for researchers, bank erosion occurs quickly compared to other geomorphic processes. However, this means that changing conditions can cause rapid decreases or increases in erosion rates that can quickly impact fluvial systems. For this reason, it is important to understand bank erosion rates and processes (Hooke, 1979).

In alluvial channels, bank erosion can occur by fluvial processes or mass failure. The term “fluvial processes” refers to picking up and transporting particles from the bank by the flow of water. The flowing water can pick up bank materials grain by grain or in small clumps. Mass failure refers to the movement of material down-slope due to gravitational forces. On a steeply sloping bank, slab failure can occur as a large portion of bank material detaches itself and falls away from the bank. Rotational failure may occur where banks slopes are shallower, when bank material slides down along a curved failure plane. Bank failure may also occur when grains or small clumps of grains fall down the face of the bank. Undercutting of stream banks can occur where weaker bottom layers erode out from underneath stronger layers, eventually causing the upper layers to topple over (Charlton, 2008).

Pre-weakening conditions include extreme saturation or drying of bank soils (Charlton, 2008), and pre-weakening processes can include anything that causes fluid pressure changes within the soil pores (Thorne and Osman, 1988), cracks to form, or the soil structure to be altered (Charlton, 2008). For example, as pore water dries out, suction forces increase between the particles, increasing the resistance to bank erosion. As drying continues, bank erosion rates can also increase as the shrinking of clumps of sediment causes cracks at the surface of the bank, which cause the bank to erode more easily (Charlton, 2008). Extreme saturation can also act as a pre-weakening process when excess water decreases bank stability, leading to mass failure. Another pre-weakening process occurs when air becomes trapped within pores by high floodwaters and pressure within the pores causes movement of bank materials in a process called slaking (Thorne and Osman, 1988). Temperature changes within the banks can also cause pre-weakening as it may affect pressure within pores or cause ice to form altering the structure of the bank face.

1.2 Factors that Affect Bank Erosion

Bank erosion may be strongly influenced by: riparian vegetation (Pizzuto and Meckelnburg, 1989; Wynn et al., 2003), bank material strength (Hooke, 1979), near-bank velocity (Leopold and Wolman, 1960), and freeze-thaw cycles (Gatto, 1995). All four influences have either a direct impact on fluvial processes or mass failure, are a pre-weakening process, or lead to conditions that cause one of these. Freeze-thaw cycles influence pre-weakening processes and mass failure (Gatto, 1995), near bank velocity influences fluvial processes (Leopold and Wolman, 1960), and bank material strength and riparian vegetation influence all three (Hooke, 1979; Wynn et al., 2003).

1.2.1 Riparian Vegetation

Riparian vegetation can have a large influence on bank stability. Whether the vegetation causes an increase or decrease on bank erosion depends on characteristics of the vegetation including root density, root depth, and characteristics of the plants themselves (Wynn et al., 2003). Vegetation that extends into the flowing water can create resistance decreasing water velocity, which can cause a decrease in the erosive power of fluvial forces (Thorne and Furbish, 1995). The roots of riparian vegetation can also slow erosion by holding the soil in place. The extent of this decrease depends on spatial factors related to root depth and bank height. For example, a tree with a taproot extending down the entire vertical bank face will be more successful at decreasing bank erosion than shorter roots like those of small grasses. Root density is also important, since for two banks with similar characteristics, the bank with a higher root density would have a lower erosion rate (Wynn et al., 2003; Pizzuto and Meckelnburg, 1989). Roots growing through soil can also create more pore space increasing drainage ability and therefore erosion because of excessive drying (Charlton, 2008). The increased pore space may also increase the effects of freeze-thaw cycles as more water can be held within the bank pores to form ice.

1.2.2 Near-bank Velocity

Near-bank velocity refers to the velocity of water at the location adjacent to the eroding bank. In a straight channel, velocity follows a set distribution of flow with the highest stream velocities located in the center of the channel (Charlton, 2008). Channel curvature will alter this distribution causing the locations of the highest and lowest flow velocities to change. On a meander bend, the location of highest velocity will shift from the center of the channel to the outside edge of the channel bend. The high velocity flow will stay along the edge slightly past the apex of the bend and wander back and forth, following the outside edge of the meander bends (Leopold and Wolman, 1960). The greatest velocity will occur near the outside of a meander slightly downstream from the meander's apex. It is likely that in these areas of high near-bank velocity, there are higher relative erosion rates because there is a higher fluvial force exerted on the banks in this area.

1.2.3 Bank Material Strength

Bank material strength consists of two basic aspects: the bank material's erodibility and the bank's shear strength. Erodibility is the bank's ability to be affected by channel flow. Bank material shear strength is the bank's ability to resist deformation due to gravity, such as bank slipping or slumping (Thorne 1981). This shear strength depends on environmental conditions and properties of the material itself (Charleton, 2008). Properties of the material can include particle packing. The tighter they are packed, the more contact there is between individual grains, which increases the amount of friction between them, and therefore increases the shear strength. Cohesive forces, like those between silt or clay particles can also increase shear strength, and cohesion can be altered by changes in soil saturation or even roots of plants. Other properties can include pore water pressure which can alter the shear strength through changing the frictional resistance between particles. Particles can be forced apart as saturated pores develop a positive pore water pressure. This saturated state causes a reduced frictional resistance, and therefore a reduced shear strength. When the bank material dries, negative pore water pressure develops and particles, especially silt and clay, are held together by suction forces. This increases frictional resistance and therefore increases shear strength in the bank (Charleton, 2008).

1.2.4 Freeze-thaw Cycles

Freeze-thaw cycles have a strong influence on bank erosion rates in colder regions where ice crystals, needles, wedges, and lenses can weaken bank material, as pore water periodically freezes and melts (Lawler, 1988). This process occurs when the air temperature dips below freezing and the ground loses heat to the air until soil water within the bank starts to freeze. The frozen water can separate and reorient soil particles as it freezes. Suction forces draw an increasing amount of water to the freezing soil zone, to the point where there may exist more water frozen within the region than there was in the soil prior to freezing. When temperatures rise and the ice thaws, the soil not only has a disrupted soil structure but also has an excess of soil water making the banks much more likely to collapse by mass failure or be eroded by currents, rain, or overland flows (Gatto, 1995).

Bank characteristics that affect freeze-thaw cycles include bank material, canopy cover, aspect, and soil moisture (Gatto, 1995). Bank material determines pore size, and it is expected that larger pores connected to the surface or bank face enhance freeze-thaw processes, because of the greater available space for water and ice to fill. Canopy cover and aspect determine shadowing affects and therefore the potential for spatially distributed differences in bank temperature. A lack or excess of soil moisture can change the rate of freezing. Temperatures in the area frequently dip above and below freezing in winter months, and therefore freeze-thaw effects are expected to increase bank erosion rates dramatically (Merritts et al., 2011; Oberholtzer, 2011; Pizzuto and O'Neal, 2009).

1.3 Approaches to Measuring Bank Erosion

The methods for measuring bank erosion rates in this study include the use of historical aerial imagery and exposed tree root dendrochronology. Other methods for measuring bank erosion include using erosional pins, repeat cross sectional surveys, or LiDAR surveys, but these techniques can require expensive equipment, disrupt the banks, or may only measure short term erosion rates, which may not be appropriate if rates have changed over time. By using aerial imagery, an entire eroding portion of a bank can be analyzed, and where aerial images are easy to obtain, the process is rather quick and inexpensive. Depending on the available historical imagery, erosion rates can be found for decadal timescales. Tree root analysis is a rather inexpensive method that can detect bank erosion in areas with suitable riparian vegetation or very low bank erosion rates, where aerial imagery may not prove effective (Stotts et al., 2014).

1.3.1 Historical Aerial Imagery Analysis

Analysis of historical aerial images is useful where images can be obtained for two different years and when the bank edges can be identified in both images. Once two images are georeferenced with GIS techniques and bank lines are drawn successfully, a polygon between the old and new bank lines can be drawn, which represents the area eroded between the time that the two images were taken (Rhoades et al., 2009). It is important to know that the meander bend has been migrating in the same general direction during this time in order to properly predict an area of erosion.

1.3.2 Tree Root Dendrochronology

Dendrochronology is the science of dating trees based on annual growth rings in order to learn something about the environment in which they grow. Tree roots can be used to determine erosion rates because a root's anatomical structure differs depending on whether it is exposed to the atmosphere and therefore acting as stem wood or buried and therefore acting as root wood. A tree root can change this anatomical structure if the conditions in which it grows changes, for example if a once-buried root becomes exposed. When a root is exposed there may be specific indicators or markings that can show how long ago this change occurred. Although past studies have focused primarily on conifer trees, any tree that displays seasonality in its rings can be used (Gartner et al., 2001; Stotts et al., 2014; Fayle, 1968).

To quantify erosion rates, the year of root exposure and the current distance away from the bank material is determined. There are many potential indicators of exposure to look for when analyzing the exposed roots. The year of exposure can be indicated by exposure scars created by high flow events where the root is damaged by flowing debris. This could occur at the first year of exposure or during other later events. Uneven formation of annual rings might indicate a time of uneven pressure exerted on the root. This may occur when one side of the root is exposed, and the rest is still within bank sediments. Rings that grow after exposure may show a change in vessel or cell size or a dramatic increase or decrease in ring widths. Bending rays which typically run straight and perpendicular through annual rings may indicate exposure as well. There may be changes in cell and vessel arrangement, for example, if the vessels started out evenly spaced, but after exposure they concentrate to the outside of the ring. If more than one of these indicators are present and they point to the same year, it can be assumed that this was the year of exposure (Gartner et al., 2001; Stotts et al., 2014). A study by Corona et al. (2011) showed that on average a root will show signs of exposure once erosion reduces sediment cover to about 3.0 cm.

1.4 Objectives of this Study

This river bank erosion study contributes to a larger sediment transport study in the White Clay Creek watershed, one of four primary watersheds in the Christina River basin. The sediment transport study will create a sediment budget and use transport models to quantify the timing and spatial extent of effects related to sediment restoration projects. Researchers will map and quantify rates of erosion and deposition and use dating methods to find particle residence times. This information will be used to create a sediment transport model for the White Clay Creek watershed that includes the often-overlooked alluvial storage times. This new model will be able to predict the amount of time necessary for restoration projects related to excess sediment to have the desired beneficial outcome and determine where in the watershed future restoration projects will have the largest benefits. A current large-scale restoration project in the East Branch of the White Clay Creek will give an opportunity for researchers to first test the model.

The goal of this river bank erosion study is to provide one component of the sediment budget for the White Clay Creek watershed by quantifying the rates of stream bank erosion and factors that control bank erosion rates. At carefully chosen field sites, bank erosion rates were estimated using historical aerial imagery and exposed tree root analysis while considering bank erosion controls that include riparian vegetation, bank material strength, and near-bank velocity, while other researchers have begun to study freeze-thaw cycle processes. The results of this project can be used to estimate bank erosion rates for the entire White Clay Creek watershed.

The objectives of this study were to;

1. Quantify bank erosion rates by tree root dendrochronology and historical aerial image analysis at representative sites in the White Clay Creek watershed,

2. Measure variables controlling bank erosion at each study site, focusing on riparian vegetation, bank material strength, and near-bank velocity, so relationships can be developed to predict bank erosion rates at any location within the White Clay Creek watershed.

Chapter 2

STUDY AREA

2.1 Location

The study area is the upper White Clay Creek watershed of which 45% is located in New Castle County, Delaware; 55% in Chester County, Pennsylvania; and less than 1% in Cecil County, Maryland. It spans 279.2 km^2 (Narvaez & Homsey, 2016) and is one of four primary watersheds in the Christina River basin, a part of the Delaware River basin. The East, Middle, and West Branches of White Clay Creek combine and later Middle Run, Pike Creek, and Mill Creek join as tributaries before it exits at the southeastern side of the watershed and enters the Christina River. The 2016 White Clay Creek Watershed Report states that 37% of the watershed is of urban land use (mostly in Delaware), 33% is used for agriculture (mostly in Pennsylvania), and 30% consists of forests and wetlands (Narvaez & Homsey, 2016).

2.2 Stream Gaging Stations

All but one eroding bank sites used in this study are located upstream of a USGS gaging station near Strickersville, PA (USGS station # 01478245). This drains a 153.3 km^2 watershed and has records for 25 years of discharge data as well as 5 years of turbidity and suspended sediment discharge data. Another USGS gaging station is located further upstream on the East branch of the White Clay Creek in Avondale, PA (USGS station # 01478120). Here the watershed has a drainage area of 29.3 km^2 which includes six eroding banks used in this study. The Avondale stream gage measured water discharge for the last ten years. The Stroud Water Resource Center has discharge data for the past 46 years further upstream in the East Branch of White Clay Creek upstream of Avondale, PA, near where three eroding bank study sites are located.

Figure 2.1. A map depicting the Christiana watershed including the four main sub-watersheds of which the White Clay Creek is one.

2.3 Geology

The watershed is located on both sides of the Fall Line, which separates the rocky Piedmont from the sandy Atlantic Coastal Plain (Narvaez & Homsey, 2016). Channels that span no more than 55 meters across take on a variety of characteristics; for example, some reaches can be considered bedrock streams (Turowski et al., 2008) that flow between very steep valley sides and others may be called alluvial and are surrounded by wide floodplains. Bed material includes very fine sand and clays to larger cobbles and boulders. Stream banks are varied in height and slope, some reaching straight upwards and some lined with shallow sloping point bars. Eroding banks are often tall vertical structures with faces of bare soil and exposed roots from vegetation at the top of the bank. Some erosional sites throughout the watershed have exposed stratigraphic units similar to those described by Jacobson and Colman (1986) in Maryland.

2.4 Climate

The watershed is located near the coast of the mid-Atlantic U.S. and can therefore be classified as humid and subtropical with four defined seasons that include hot, humid summers and mild winters. This region can join the southern U.S. and receive hurricanes, but also occasionally join the North in receiving nor'easters (Mogil and Seaman, 2009). The town of Avondale, PA (located in the northern half of the watershed), has an average January low temperature of -5.7° C and an average July high of 28.5° C. In Newark, DE, in the mid to southern portion of the watershed, the average annual rainfall is 117.3 cm and average annual snowfall is 20 cm http://www.usclimatedata.com/climate/newark/delaware/united-states/usde0043, accessed 01/16/2017).

2.5 Site Selection

Seventeen eroding banks within thirteen stream reaches were chosen. This includes an eroding bank at sites 1, 2, 3, 4, 5, 6, 8, 9, 10us, 10mid, 10ds, 11us, 11mid, 11ds, 12, 14, 16, of which 10us, 10mid, 10ds are within the same reach and 11us, 11mid, 11ds are within the same reach. The upstream and downstream coordinates of the ends of each eroding bank, as well as the Strahler stream order is reported in Table 2.1.

Table 2.1. A table reporting the upstream and downstream coordinates of the ends of the studied eroding banks and the Strahler stream order

Site	Upstream Coordinates	Downstream Coordinates	Stream Order
1	39°44'56.05"N, 75°46'10.51"W	39°44'53.17"N, 75°46'11.51"W	4
2	39°43'46.59"N, 75°45'38.07"W	39°43'46.82"N, 75°45'42.40"W	4
3	39°47'12.89"N, 75°49'9.44"W	39°47'11.48"N, 75°49'7.68"W	2
4	39°45'46.02"N, 75°46'1.41"W	39°45'42.94"N, 75°46'2.69"W	3
5	39°46'7.06"N, 75°45'47.04"W	39°46'4.82"N, 75°45'48.90"W	3
6	39°47'11.19"N, 75°46'23.23"W	39°47'10.67"N, 75°46'24.52"W	3
8	39°48'13.29"N, 75°49'48.16"W	39°48'13.52"N, 75°49'46.61"W	2
9	39°48'52.09"N, 75°46'57.65"W	39°48'50.48"N, 75°46'58.95"W	3
10us	39°51'23.30"N, 75°46'57.68"W	39°51'23.28"N, 75°46'59.30"W	2
10mid	39°51'21.76"N, 75°47'0.89"W	39°51'20.93"N, 75°47'1.60"W	2
10ds	39°51'18.25"N, 75°47'4.29"W	39°51'18.01"N, 75°47'3.25"W	2
11us	39°51'35.68"N, 75°47'4.04"W	39°51'34.78"N, 75°47'3.89"W	2
11mid	39°51'34.74"N, 75°47'4.09"W	39°51'33.99"N, 75°47'2.43"W	2
11ds	39°51'34.08"N, 75°47'2.40"W	39°51'33.32"N, 75°47'1.43"W	2
12	39°45'26.38"N, 75°47'2.73"W	39°45'25.59"N, 75°47'5.69"W	3
14	39°47'8.30"N, 75°48'10.38"W	39°47'5.64"N, 75°48'9.86"W	2
16	39°48'26.98"N, 75°45'19.36"W	39°48'26.56"N, 75°45'19.37"W	1

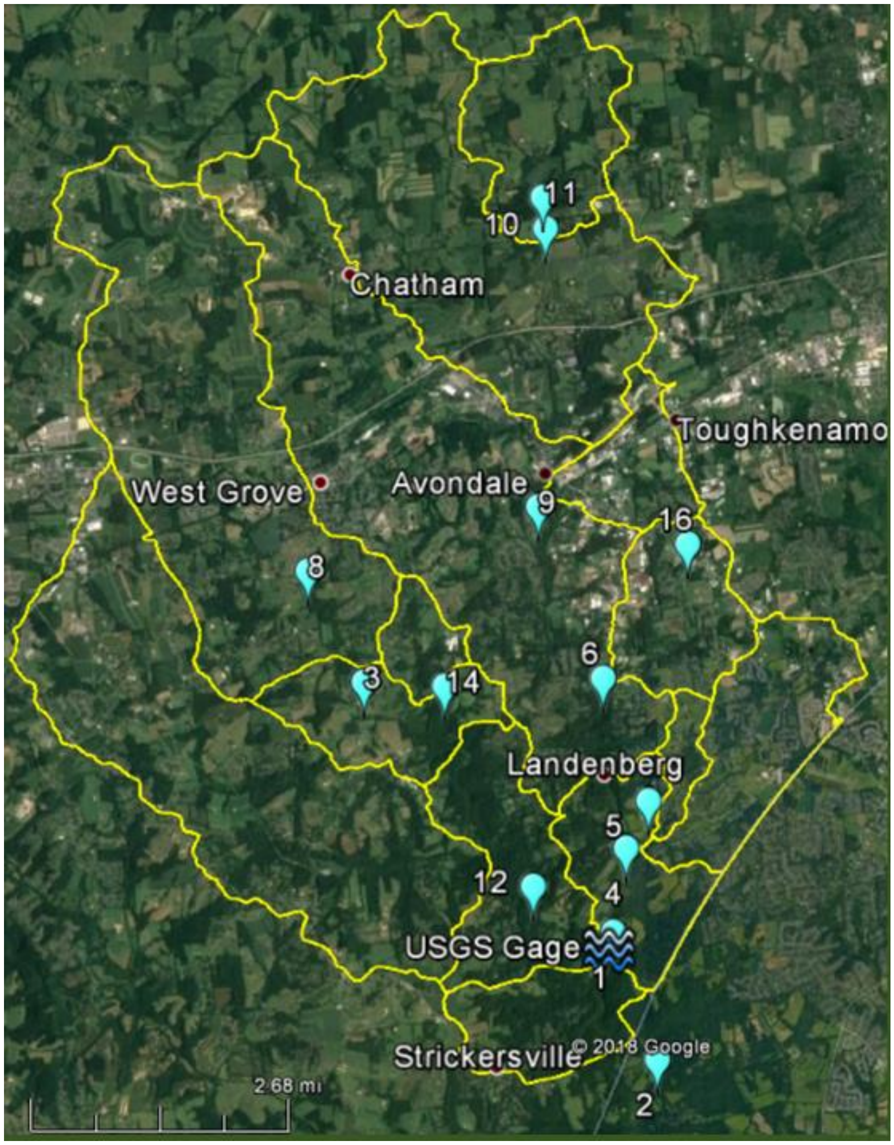

Figure 2.2. A map depicting the Pennsylvania portion of the White Clay Creek watershed including the 13 reaches in this study and the USGS gage at Strickersville, PA.

Chapter 3

METHODS

The methods carried out in this study were completed to either quantify erosion rates, measure controls to bank erosion, or provide a general geomorphic picture of the specific stream reach. Because many data sets were collected to complete this study, a flowchart of which data sets contribute to each major objective is depicted in Figure 3.1.

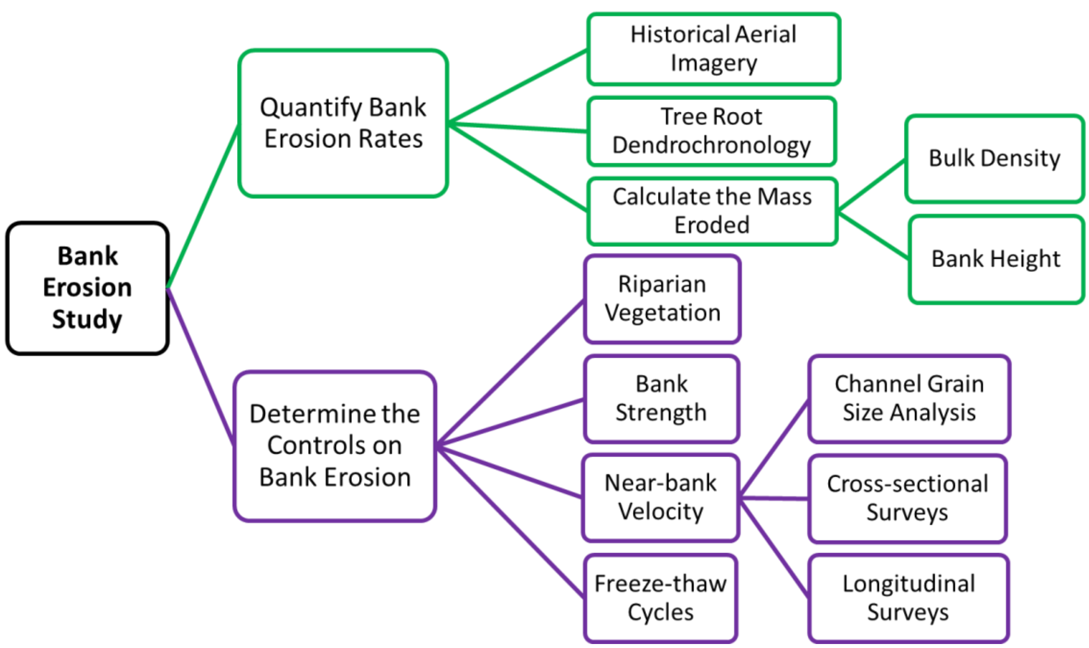

Figure 3.1. A flowchart depicting the two main objectives and data sets required to complete each of the objectives.

3.1 Site Selection

Thirteen stream reaches covering 17 eroding banks were chosen with varying stream order (Strahler, 1957), tree cover, and channel curvature. Sites 2, 10, and 11 were chosen because there had been geomorphological data collected at these sites in the past. TLS and CRDP surveys have monitored the meander and adjacent point bar for erosion and deposition over three years at Site 2 (Cribb, 2017). A study on the reaches that include sites 10 and 11 included estimating bank erosion rates by aerial imagery at site 10 and tree-root dendrochronology at site 11 (Williamson, 2013). All reaches except site 2 are located in the Pennsylvania portion of the watershed upstream from the USGS gaging station near Strickersville, PA. Site 2 is located just downstream of the Pennsylvania-Delaware border. Site 16 is the only first order stream, sites 1 and 2 are fourth order streams, and the rest are second or third order according to the map in Figure 1 of the White Clay Creek State of the Watershed Report: 2008 (Corrozi, M. et al., 2008).

At each study reach, one eroding bank was identified and chosen, except at sites 10 and 11 where three eroding banks were chosen at each. Some eroding banks were first identified by rapid changes in channel planform observed from comparing historical aerial images and others were identified directly in the field. To be identified as an eroding bank, the banks had to be close to vertical and no vegetation growth (besides the occasional cluster of moss) could be growing on the exposed bank face. Examples of eroding banks identified in this study can be seen in Figures 3.2, 3.3, and 3.4.

Figure 3.2. An image depicting the eroding bank at site 2, the stream with the highest drainage area.

Figure 3.3. An image depicting some eroding banks at site 16, the lowest order stream.

Figure 3.4. An image depicting the eroding bank at site 12, a third order stream.

3.2 Geomorphic Mapping and Bank Descriptions

At each site, notes were taken on major features within the stream reach. Features mapped include large boulders, bedrock exposures within the channel boundary, tributaries, in-channel bars, point bars, large woody debris, noteworthy vegetation, pools and riffles, qualitative channel bed grain size observations, high water channels, and types of human influence. Eroding banks were identified as eroding through either alluvial or colluvial material based on observations of sediment sorting and roundness. The geomorphic maps were used to verify locations of eroding banks, cross sections, and sampling locations. Results of channel depth and velocities given by Matlab code results described in later sections were compared to the basic observations in the geomorphic maps to confirm the existence of pools, riffles, and locations of potential erosion or deposition.

Bank face stratigraphic descriptions were completed at each site which included an estimated description of sediment grain size, sedimentary structures, layer thickness, and color. A thin layer of material was scraped from the bank leaving an exposed face, and different stratigraphic layers were identified and measured. Observations were recorded for the type of material with an estimate of percent mud, sand, and gravel. The color at each layer was determined by comparing the material to color swatches in a Munsell soil color chart and roots, mottles, boulders, and other sedimentary structures were recorded as well.

3.3 Surveying

3.3.1 Cross-sectional Surveys

Cross-sections were surveyed using a Topcon Electronic Total Station at a location close to the eroding bank but where the planform was less curved and therefore the channel cross section was relatively symmetrical. At locations like these it can be assumed that the near-bank velocity along the two adjacent banks is about the same. Care was taken to record a survey point at relatively large changes in slope, the edges of the water on each bank, and at locations of significant changes in sediment size. All surveyed points were separated by no more than one to two meters. For sites 10us, 10mid, and 10ds a single cross-section was taken from Elise Williamson's data. The same applies to sites 11us, 11mid, and 11ds (Williamson, 2013). A bankfull stage was determined from each survey, and calculations were made of average depth, channel width, cross sectional area, and wetted perimeter (all at bankfull stage). Observations of changes in sediment grain size indicated the difference between the channel bed and banks, and calculations were made for the average depth above the channel bed material.

3.3.2 Surveys of Longitudinal River Profiles

The water surface slope and bed morphology were quantified using the Topcon Total Station. At each site, points were surveyed in the stream bed and at the water surface. Surveys began at the downstream end of the eroding bank and proceeded upstream for about 15 to 40 channel widths for larger order streams and up to 200 channel widths for smaller order streams. Survey points were recorded as close to the river's thalweg as possible and where the thalweg couldn't be determined, close to the center of the channel. Points were plotted and a best fit line for the water surface slope was generated. The water surface slope for most sites was confirmed with ArcGIS using digital elevation models.

Sites 6 and 8 were frozen when surveying was planned so GIS techniques to find the water surface slope are reported instead. For sites 10 and 11 the slope was reported as 0.0059 for site 10 and 0.0056 for site 11 by scientists at the Stroud Water Research Center (M. Daniels, personal communication, February 6, 2018). Because of the small size of Site 16, finding slope by DEM was impossible and a typical survey of the top of water over estimates the slope. Therefore, the change in elevation was determined by the typical survey methods, but the length of the surveyed reach was determined from Google Earth and a more reasonable slope of 0.0096 is reported.

3.4 Bank Erosion Rates

Rates of linear bank retreat were determined at each eroding bank in order to obtain a mass of sediment eroded from the river bank per year. Historical aerial imagery analysis was performed where banks could be located in the images and tree roots were scarce or too small to sample. Tree root dendrochronology was performed to find bank erosion rates at sites where exposed tree roots were plentiful and aerial images proved ineffective. The average bank height and bulk density of the bank material was determined as explained in later sections and used to find the volume and mass of sediment eroded per year.

3.4.1 Historical Aerial Imagery Analysis

On reaches with no or little exposed roots, historical aerial imagery was used to determine the rate of erosion with the program ArcGIS. Using the methods of Rhoades et al. (2009), aerial images from two different years were georeferenced using no less than 10 ground control points per image. These control points included edges of signs, benches, walk ways, buildings, bridges, and roads, being sure to account for skewing due to the different angles at which the photos were taken. Stream boundaries were digitized for an earlier and later year for each site. Historical aerial images for 1937 were very easy to digitize bank lines on as were 2013 and 2015. The most success for site 3 was from an image from 2008. For site 16 the channel was very hard to see in older aerial images so the starting year of 2010 was chosen. A later year for this site was also considered since construction of the park that it is located in seems to have affected the planform of the stream. Sites 10 and 11 used images from 1968 and 2010 (Williamson, 2013). The bank lines were digitized at different scales depending on the size of the stream at each reach. Stream boundaries were estimated where dense canopy cover prevented easy detection from the aerial images. The area of erosion was determined for each reach by finding the area between the earlier and later image's digitized stream boundaries. Where this erosional polygon pinched out, no adjustments were needed, but where only a portion of the eroding bank was used for analysis, a line perpendicular to water flow was drawn as an end to that erosional polygon.

3.4.2 Tree Root Dendrochronology

Bank erosion rates were quantified using tree root dendrochronology at sites 1, 4, 6, 9, 12, and 14, and past tree root data collected by former master's student, Elise Williamson at sites 11us, 11mid, and 11ds were considered as well (Williamson, 2013).

Sampled tree roots were chosen because they fit four criteria:

1. The tree root was exposed, and preferably as far as possible from the face of the eroding bank.

2. The tree root appeared to be living.

3. The sampling location on the root was greater than 0.5 meters away from the stem, germination point, and/or taproot.

4. The circumference of the root was small enough that it could be easily cut and analyzed in the lab and that collecting the sample wouldn't affect the stability of the tree or bank.

5. The circumference of the root was big enough that it could be analyzed with the necessary equipment.

Using these criteria, four to eight root samples were collected at each eroding bank as seen in Figures 3.5 and 3.6. The species of each sampled tree was determined, and a tree corer was used to find the age at breast height. The tree's age was determined once the core was secured to a mount and sanded.

Figure 3.5. An image depicting exposed tree roots along an eroding bank at site 1. The sampled root is marked.

After finding GPS coordinates of the location, a disc-like sample about 5 to 15 centimeters long was cut from the selected exposed root. Its orientation was recorded including how far the left-most and right-most parts of the sample were from the eroding bank, measured level horizontally and perpendicular to water flow (Stotts et al., 2014). These distances were averaged to find the distance from the bank (E_x). A diagram of this technique can be seen in Figure 3.7.

Figure 3.6. An image depicting exposed tree roots along an eroding bank at site 9. The two root slices taken are marked.

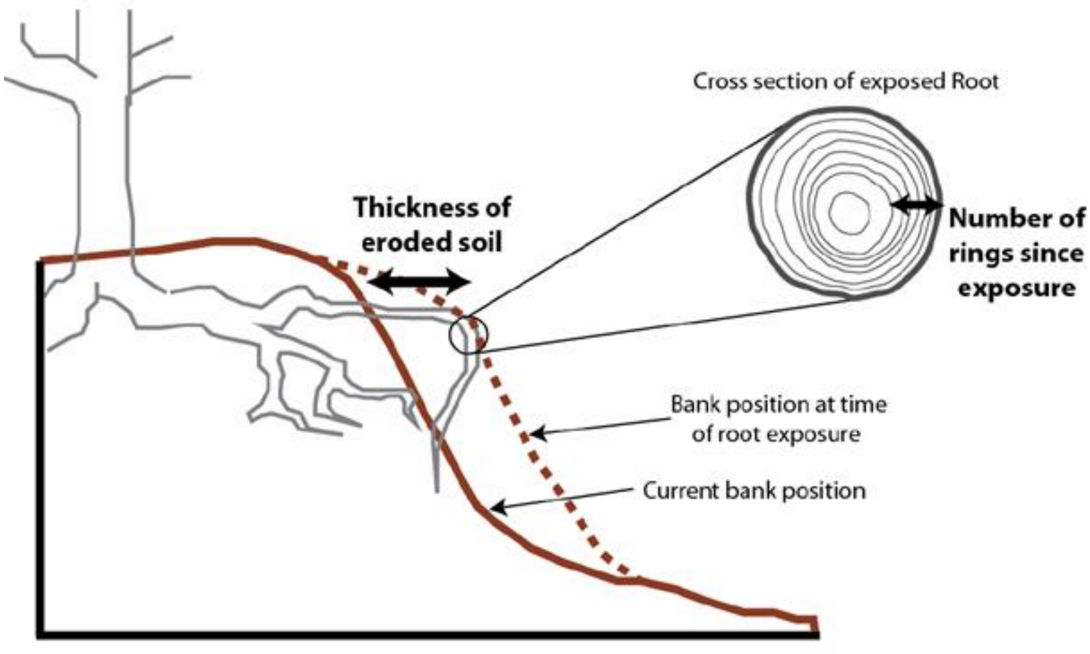

Figure 3.7. A diagram depicting an exposed root along an eroding bank showing how the bank position has changed with time, and a sample cross-section of the exposed root. Figure from Williamson (2013).

The sampled root is taken back to the lab where it is cut to fit a microtome, being sure to include in the piece the center of the root as well as the bark on at least one side. The microtome is used to slice the root sample into thin layers, and water is used to keep the root slice on a microscope slide as seen in Figure 3.8.

Figure 3.8. An image of root samples after being sliced with a microtome and prepared on microscope slides.

The slide base was constructed in a way that could move the sample left or right five micrometers at a time. The microscope used was set up with a camera projecting to a computer monitor. A perpendicular cross was drawn in the viewing window on the computer. Ring widths were measured by lining up the edge of a ring with the line on the viewer and moving the slide base until the line was at the opposite end of the ring. The length that the base had moved was recorded as the tree ring width. Observations were recorded for each ring to help identify the year of exposure. Observations included notes on color, cell size, ray alignment, vessel arrangement, variation in ring width, damage scars, and anything else of importance (Gartner et al., 2001). Once the year of exposure was identified (*NRex*), measurements were made for the average width of the bark (*B*) and the amount of radial root growth after exposure (*Gr1*). A formula used and modified by Corona et al. (2011) was used to determine the erosion rate (E_{ra}) at the location that the root was sampled:

$$E_{ra} = \frac{E_x - (Gr1) + B}{NRex}$$

This method assumes that the average bark width stays constant from the time it was exposed to present. A study by Corona et al. (2011) showed that, on average, a root will show signs of exposure once erosion reduces sediment cover to about 3.0 cm, so the formula was modified further by using a distance of bank retreat value (R_d) equal to the distance from the bank (*Ex*) minus 3.0 cm:

$$E_{ra} = \frac{R_d - (Gr1) + B}{NRex}$$

Because the sampled roots were not evenly spaced throughout the length of the eroding bank, each erosion rate was assigned to a certain length of bank around the sampled root. Where the eroding bank pinched out, that end point was given an erosion rate of 0 cm/yr. Where the end of a site does not pinch out, the end point was given an erosion rate equal to that of the closest root sampled. The calculated erosion rates found at the sampled locations were used for the length of bank halfway to the next sampling location. Then a weighted average based on distance was calculated to find the average erosion rate in area per year for the entire eroding bank. A diagram depicting this method can be seen in Figure 3.9. A weighted average standard deviation was computed for the bank erosion rates determined by the tree roots, ignoring the ends of the bank in the calculation.

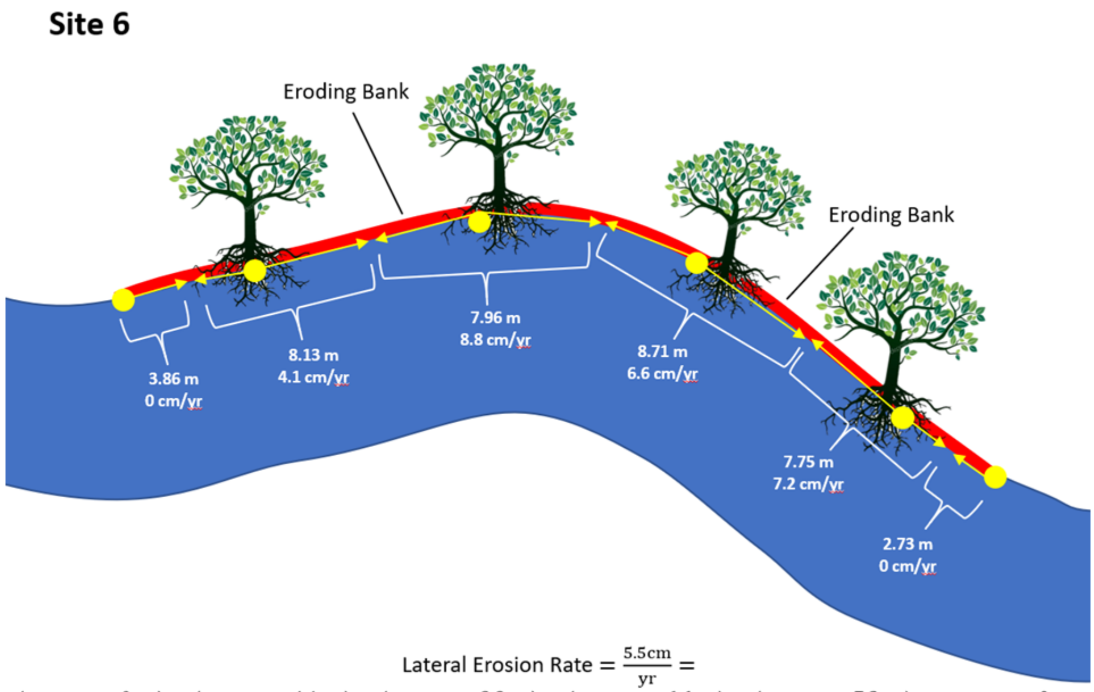

$$\text{Lateral Erosion Rate} = \frac{5.5\text{cm}}{\text{yr}} = \frac{\left(.0386cm * \frac{0cm}{yr}\right) + \left(.0813cm * \frac{4.1cm}{yr}\right) + \left(.0796cm * \frac{8.8cm}{yr}\right) + \left(.0871cm * \frac{6.6cm}{yr}\right) + \left(.0775cm * \frac{7.2cm}{yr}\right) + \left(.0273cm * \frac{0cm}{yr}\right)}{(.0386cm + .0813cm + .0796cm + .0871cm + .0775cm + .0273cm)}$$

Figure 3.9. A diagram and sample calculations used to find the bank averaged lateral erosion rates at site 6.

3.4.3 Bank Height

The average bank height was determined on GIS using a one meter digital elevation model (DEM) and it's corresponding hill shade map. Lines were drawn on a hill shade map marking the top of the water and top of the bank adjacent to the eroding bank. The elevation was extracted at every meter along the two lines and an average and standard deviation was calculated for each. The average top of water height was subtracted from the average top of bank height to get the average height of the eroding bank and a total standard deviation was calculated. The top of water was used as a proxy for the bottom of the bank since the stream reaches in this study are not very deep, especially along the edge of the banks. Bank heights could not be taken from the DEM for Site 16 due to its small size. At this site, field measurements of bank height were collected along the bank every one meter upstream and these values were averaged. It is assumed that the bank heights have not changed over time.

3.4.4 Bulk Density

The bulk density of bank material was determined for each eroding bank. At each of the layers with thickness (*w*) indicated by the bank descriptions, one to three bulk density samples were taken as described by Natural Resource Conservation Service (2017). A flat face was created by scraping a few centimeters of sediment from the exposed bank. A cylindrical ring that can hold a volume of 15.48 cm^3 was hammered evenly into the side of the bank until flush with the flat face. Care was taken to not hit the soil when hammering, in order to avoid artificially conpacting the bank material. Being careful not to lose any sediment, the ring is dug out and removed from the bank. A flat bladed knife was used to smooth the bottom and top surfaces even with the outside of the ring and any sediments stuck to the side of the ring were wiped away. The rings holding the samples were put in labeled bags and brought back to the lab. Here the sediment was placed into a pre-weighed beaker and dried in an oven. Once dry, the beakers were left to cool to room temperature and then weighed. The dry mass of the sample is calculated by subtracting the mass of the dry material and beaker by the mass of the beaker. The bulk density (ρ_b) of the bank material was then calculated as follows:

$$\rho_b = \frac{dry\ mass\ of\ sample}{volume\ of\ sample}$$

A weighted average bulk density was taken for each bank to account for the differences in layer widths as shown in the formula:

$$weighted\ average\ \rho_b = (\rho_{b_r} * w_r) + (\rho_{b_s} * w_s) + (\rho_{b_t} * w_t) + \cdots$$

where *r*, *s*, *t*, and etc. are the different bank layers. A weighted average standard deviation was calculated for each bank.

3.4.5 Calculations for Mass

Erosion rates can be reported as a mass of sediment eroded from the bank per year. Results of tree root dendrochronology and aerial image analysis are reported as areas eroded per year. The calculated average bank height can be multiplied by this rate to report a volume eroded from each bank per year. This can then be multiplied by the bulk density to report a mass of sediment eroding from the bank each year. Errors are calculated from the standard deviations of bulk density and bank height measurements, as well as from variations in tree root data.

3.5 Riparian Vegetation

Riparian vegetation density calculations were determined adjacent to each eroding bank by direct measurement in the field. At each site an area was marked out that extended five meters back from the eroding bank. All trees within this area were measured for their circumference at breast height so long as they followed the following criteria:

1. The tree's circumference was measured to be at least 30 cm at breast height.
2. The tree's trunk was located at least halfway within the assigned area.
3. For a tree or bush that forks below breast height, only the boughs that have a circumference of at least 30 cm at breast height are recorded (for data analysis purposes, these boughs' circumferences were added together).

4. The tree is living or if dead has a root system that appears to be effectively holding on to sediment in the ground.

The general location of each tree was mapped, which includes the distance from the eroding bank at each tree measured.

Calculations were then made for the density of riparian vegetation. The total tree cross-sectional area was calculated as the total tree trunk cross-sectional area at breast height. The total tree cross-sectional area was also calculated for trees whose cross-sectional trunk area at breast height was greater than 1000 cm2 (from now on called large trees). The percent trees by area was found by dividing the tree area by the total area of land that is five meters back from the bank. The same was done for large trees to get the percent of large trees by area. The tree density by number of trees was calculated by dividing the number of trees by the total area five meters behind the bank, and the same was done for large tree density by number of trees.

3.6 Near-bank Velocity

In the White Clay Creek eroding banks occur along the outside of bends as expected, as well as on straight reaches or occasionally along the inside of bends. Since erosion depends on fluvial processes, it is important to know the velocity of water that is adjacent to these eroding banks. Near-bank velocity was therefore calculated for the entire length of the eroding bank and an average near-bank velocity along each eroding bank was determined. This was completed using a Matlab code provided by Ottevanger et al. (2013) through the OpenEarth repository (https://publicwiki.deltares.nl/display/OET/OpenEarth).

Model inputs include hydraulic radius, bankfull channel width, and slope, all of which were measured through the survey techniques described earlier; D_{90} which was measured in the field; water discharge and a friction factor, both of which were calculated in formulas derived by Dr. James Pizzuto; and the total length of the reach to be modeled found by using a combination of GIS and alterations of the Matlab model.

The grain size of sediment was measured in the channel bed. A gravelometer was used as a standard way to measure the intermediate axis of the grains. Starting upstream from the eroding bank a grain was picked up at random about every meter along the thalweg, or where this was unclear, the center of the channel. The grain size category was recorded, and this procedure continued until samples were taken adjacent to the downstream end of the eroding bank and there were at least 100 samples. Data was plotted in the form of grain size category versus cumulative percent of grains in each category and calculations were made for D_{90}, the grain size at which 90% of grains are smaller.

The friction factor (C_f) was calculated at each site using the derived formula:

$$C_f = \frac{n^2 g}{R^{\frac{2}{3}}}$$

where g is the velocity due to gravity, R is the hydraulic radius, and n is Manning's n which was calculated by:

$$n = \frac{(3D_{90})^{\frac{1}{6}}}{\alpha_r g^{\frac{1}{2}}}$$

Calculations were made for α_r based on data collected from site 5 using the equation above and using 0.03 as a prediction for Manning's n so that it can never be less than 0.03. The discharge (Q) was calculated by:

$$Q = URW$$

where R is the hydraulic radius at bankfull, and W is the bankfull width, and U is the velocity calculated by:

$$U = \sqrt{\frac{gRS}{C_f}}$$

where S is the slope.

Centerlines were drawn in ArcGIS based on a one meter DEM and it's corresponding hill shade map of the watershed. The centerlines extended upstream between 39 and 160 channel widths from the upstream end of the eroding bank and between 9 and 63 channel widths downstream of the downstream end of the eroding bank depending on the size of the stream reach at that location. In GIS the centerlines had to be converted to a set of coordinates every one to five meters downstream, depending on the size of the site. The model turns these coordinates into a set of points based on the length from the upstream end of the modeled reach.

A set of points marking the centerline from the top of the reach to the upstream portion of the bank and another from the top of the reach to the downstream portion of the eroding bank, were loaded into the model to find the distance downstream from the top of the reach to the two ends of the banks.

The program produces a calculated velocity field for the entire reach. After determining which side of the reach the eroding bank was located, the velocity at only the bank edge from the upstream to downstream end of the eroding bank was extracted and averaged. A standard deviation was calculated as well.

3.7 Bank Material Strength

The bank strength was measured at each bank using a dial indicating torque wrench. After clearing a sample location, a 60 x 120 mm vane was pounded into the bank the same amount at each location. At each bank ten to twelve measurements were taken as seen in Figure 3.10, spread vertically up the bank and horizontally throughout. At site 16 only six samples were taken because of its small size and the potential for sampling to negatively affect the stability of the bank. The location along the bank, the height down from the top of the bank, and a short description of the surrounding sediment was recorded. The bank strength was averaged at each site and a standard deviation was calculated.

Figure 3.10. An image showing the use of a dial indicating torque wrench for measuring bank strength on the eroding bank at site 12.

Chapter 4

RESULTS

4.1 Bank Descriptions

Bank descriptions reveal three main types of eroding banks and three other unique types. Data describing the three main types of eroding banks can be found in Figures 4.1, 4.2, and 4.3.

Sites 4, 11, 12, 14, and 16 all follow a fining upwards trend that starts with a sandy material at the base of the bank and fines up to a sandy mud. These sites have roots down at least half of the bank face and mottles that appear on the bottom portions of the bank. These banks have between 4 and 6 distinct stratigraphic layers and include sediment colors such as yellowish brown, gray brown, and olive gray. An example of this bank type can be seen in Figure 4.1 of site 14.

Sites with a muddy basal layer include sites 2, 8, 9, and 10. These muddy layers range from 11 to 58 cm thick. Above this muddy layer are layers of sandy mud, and at sites 2 and 8 the upper layer consists of muddy sand. Sites 2 and 9 include a thin (2 to 4 cm) layer of muddy sand within the sandy mud layer. Roots are located in the upper portions of these sites except at site 9 where roots span the entire height of the bank. An example of this bank type can be seen in Figure 4.2 of site 10.

Sites 1, 3, 4, and 14 have a basal layer of pebbles and cobbles in a sandy matrix with the occasional boulder that extends into the layer above. These layers range from 5 cm to 11 cm thick and are topped with layers of muddy sand and sandy mud. Mottles are located on the bottom half of all four of these banks and roots stretch to the bottom half but not all the way down the bank. An example of this bank type is shown in Figure 4.3.

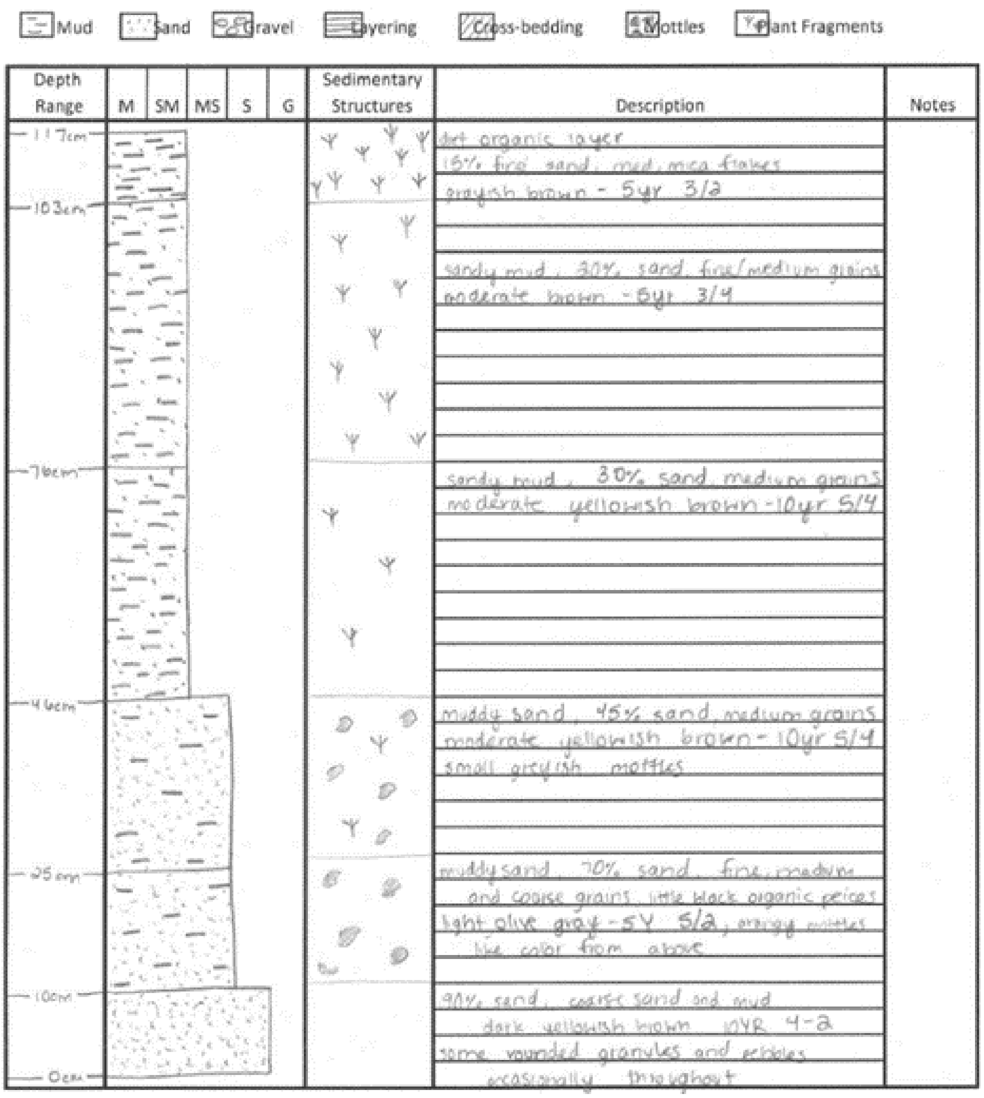

Figure 4.1. Field notes taken at site 14 showing the height of the eroding bank, mud, sand, and gravel content, sedimentary structures, color, and other notes. This bank description shows a fining upwards trend typical of five eroding river banks in the study.

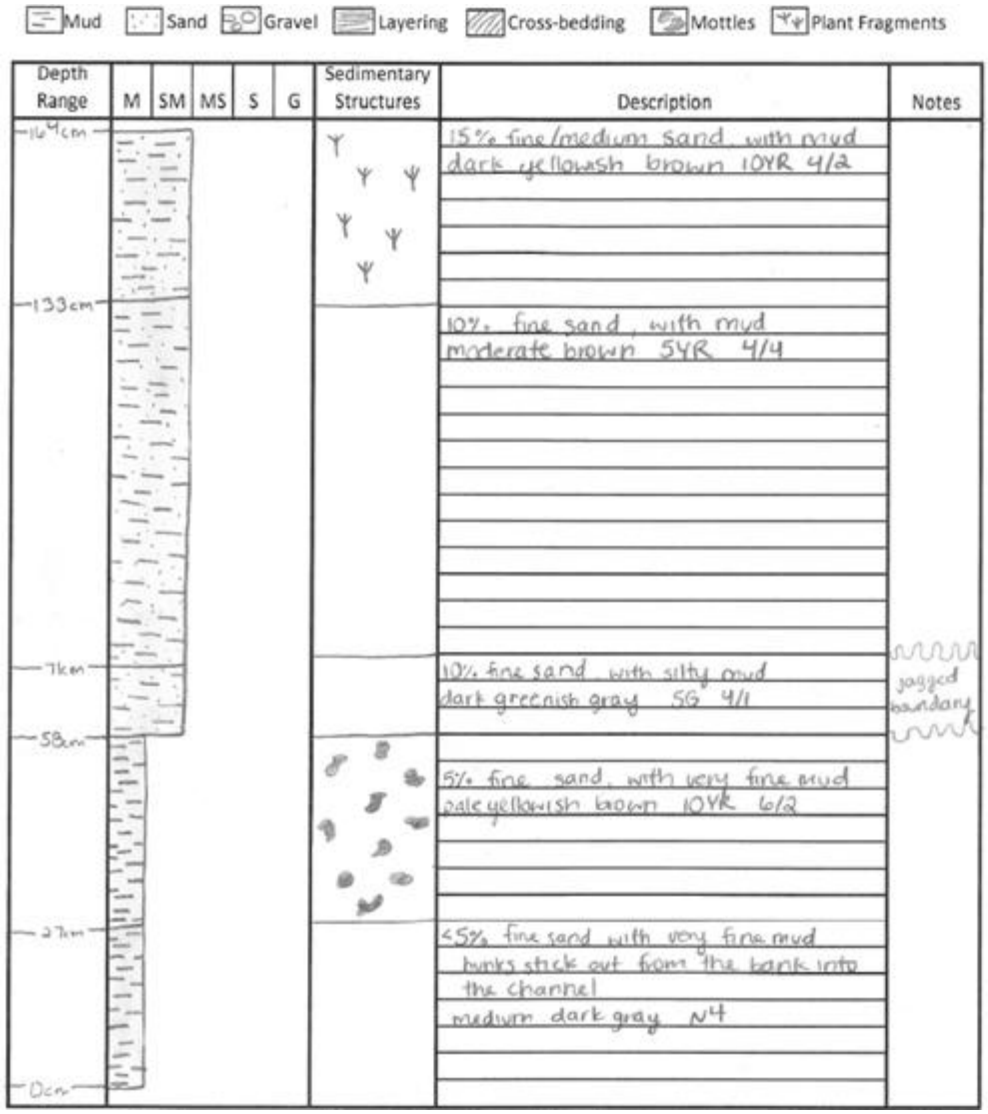

Figure 4.2. Field notes taken at site 10 showing the height of the eroding bank, mud, sand, and gravel content, sedimentary structures, color, and other notes. This bank description shows a basal layer of mud typical of four eroding river banks in the study.

Although banks at sites 5, 6, and 12 follow some of these trends, they are fundamentally different. At site 5 the bank varies greatly with distance downstream. Below a muddy sand top soil, there are three distinct layers of muddy sand, the top

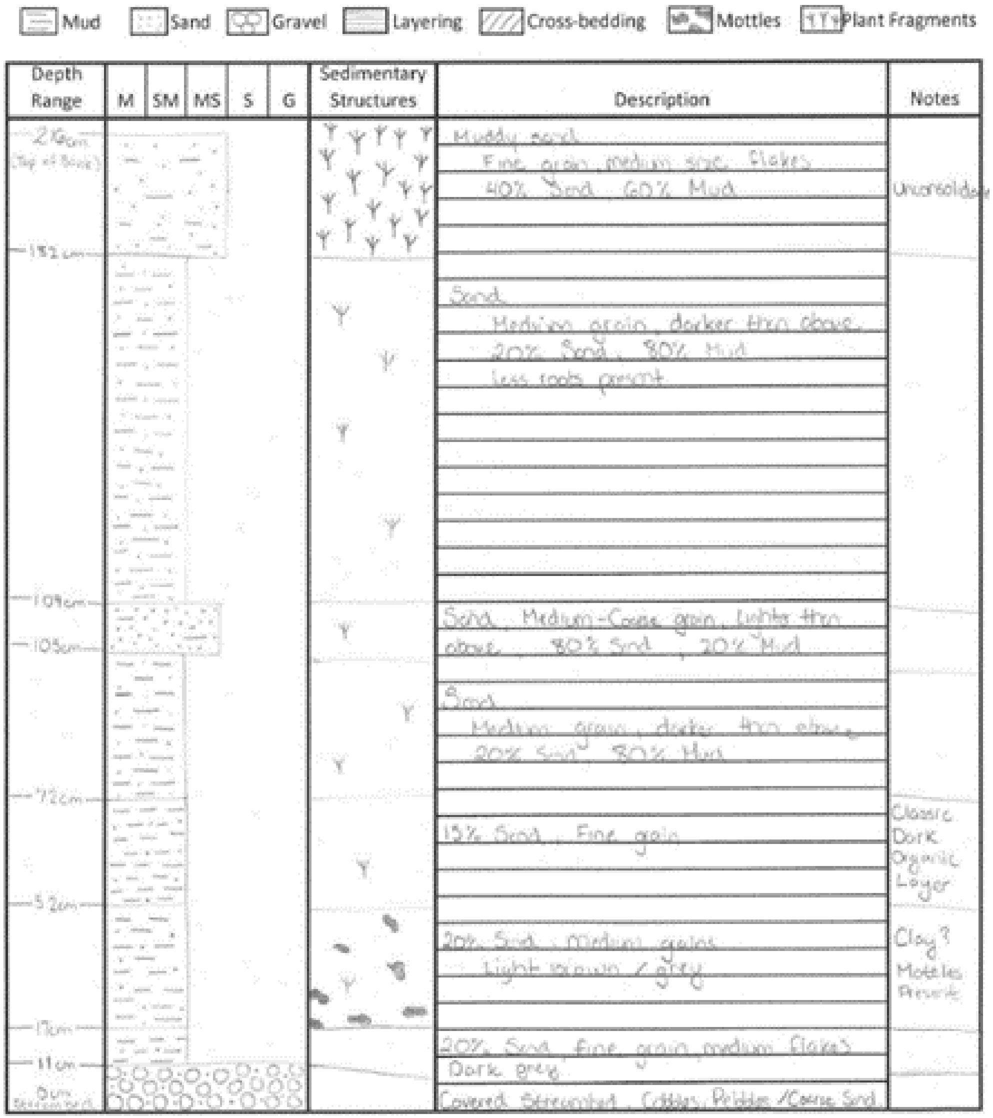

Figure 4.3. Field notes taken at site 1 showing the height of the eroding bank, mud, sand, and gravel content, sedimentary structures, color, and other notes. This bank description shows a basal layer of gravel typical of four eroding river banks in the study.

two of which include the occasional matrix supported granule, pebble, or boulder. The lowest of these layers has small multi-colored mottles throughout. The layer below this consists of varying layers of sandy mud and muddy sand and at the base there is about 80 cm of gravel, consisting of mostly matrix-supported pebbles, cobbles, and boulders. The bank at site 6 has two layers. The bottom layer consists of about 98 cm of boulders in a matrix of mud and sand. It appears clast-supported with clasts ranging in size from 25 cm to 130 cm. The top layer is about 70% muddy fine to medium grained sand and 30% boulders ranging from about 25 cm to 90 cm. Roots appear throughout this top section. The eroding bank at site 12 varied from mostly layered mud and sand near the downstream portion of the bank to areas of mostly large boulders and bedrock near the upstream portions of the bank. The upstream portion includes a thick layer of stratified and folded colored sands and muds (Figure 4.4).

Figure 4.4. An image depicting the thick layer of stratified and folded colored sands and muds in the eroding bank at site 12.

4.2 Survey Data

4.2.1 Cross-sectional Surveys

A single cross-section was surveyed at each stream reach. Calculations of bankfull area, bankfull width, channel width and depth at bankfull, wetted perimeter, and hydraulic radius are shown in Table 4.1. Bankfull areas ranged from 0.79 m^2 for the only first order stream (site 16) to 46.76 m^2 for the fourth order stream with the largest drainage area (site 2). Sites 16 and 2 also had the smallest and largest bankfull width and wetted perimeter. Site 6 passed site 2 in channel width with a measurement of 21.92 meters. Mean channel depth at bankfull ranged from 0.54 meters for site 16 to 2.75 meters for site 1 and hydraulic radius ranged from 0.19 meters for site 16 to 1.87 meters for site 1.

The morphology of the cross-sections seemed to fit into three main categories. Site 9 shows a stream whose floodplains were almost even in height on each side (Figure 4.5). Site 3 is an example of a site where floodplains adjacent to the channel differ in elevation likely due to natural causes (Figure 4.6). Site 8 shows the typical cross section of sites that are adjacent to property highly altered by humans (Figure 4.7). At site 8 the cross-section was taken adjacent to a farm field and in others this altered material might include fill for roads or railroads. The cross-sections can also be split into two main categories based on channel width/depth ratios. Sites 1, 5, 8, 9, 11, and 14 all have width depth ratios between 4.0 and 5.5 and site 16 has the lowest at 1.1. This shows that the channel depth is deeper relative to the channel width (Figure 4.5). Sites 2, 3, 4, 10, and 12 all have width/depth ratios between 7.0 and 9.7 with site 6 having the highest at 12.3. These sites have wider and shallower channels than the others (Figure 4.6).

Table 4.1. A table reporting calculations from the cross-sectional surveys. Values include the total bankfull area, bankfull width, channel width, average channel depth at bankfull, wetted perimeter, and hydraulic radius.

Site	Bankfull Area (m^2)	Bankfull Width (m)	Channel Width (m)	Channel Depth at Bankfull (m)	Wetted Perimeter (m)	Hydraulic Radius (m)
1	45.03	22.47	11.11	2.75	23.97	1.87
2	46.76	36.03	18.57	1.92	34.85	1.34
3	14.70	15.19	10.18	1.19	15.46	0.95
4	25.10	21.03	12.08	1.50	21.71	1.16
5	32.28	21.06	10.19	2.16	22.31	1.45
6	41.50	26.49	21.92	1.78	27.83	1.49
8	19.61	14.71	8.69	1.70	15.61	1.26
9	22.86	14.57	9.82	1.80	15.98	1.43
10	5.97	9.90	6.00	0.77	10.26	0.58
11	9.37	12.75	5.00	1.15	13.52	0.69
12	40.33	30.43	12.41	1.76	31.53	1.28
14	33.49	22.45	10.00	1.90	23.34	1.43
16	0.79	3.80	0.60	0.54	4.25	0.19

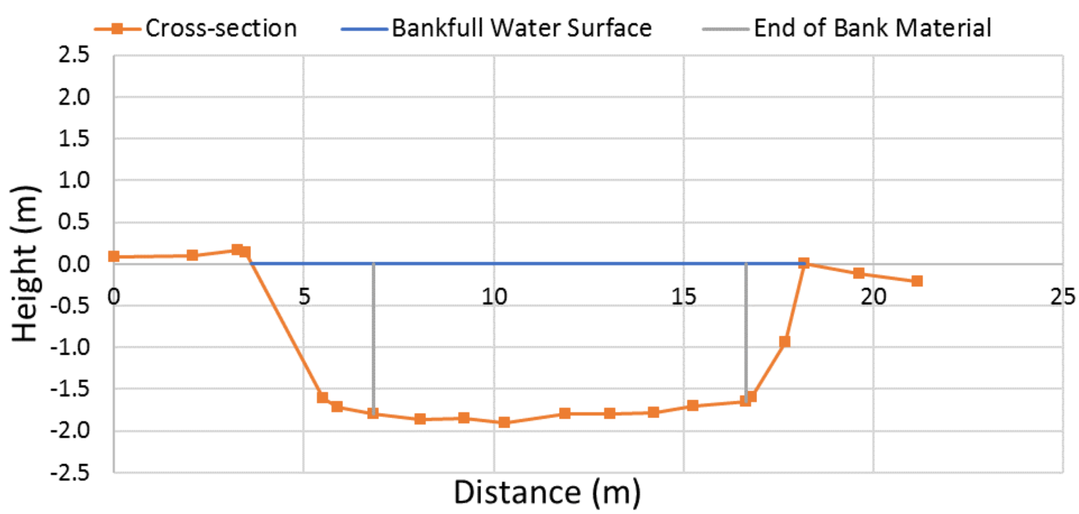

Figure 4.5. A graph depicting the river cross-section at site 9 looking upstream with a marked bankfull water surface line and ends of the channel material as observed while surveying. This is a typical cross-section where the two floodplains are the same height and the width/depth ratio is low.

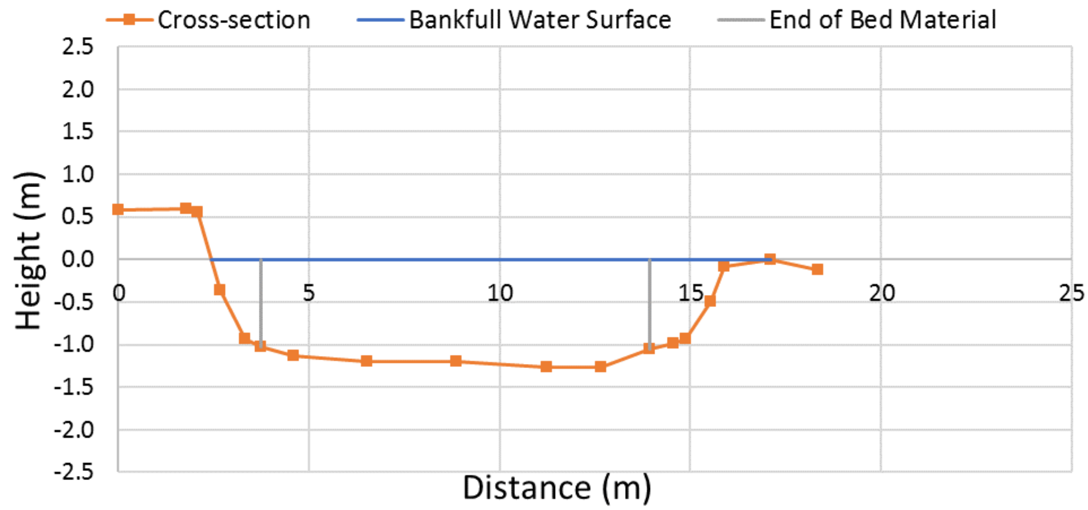

Figure 4.6. A graph depicting the river cross-section at site 3 looking upstream with a marked bankfull water surface line and ends of the channel material as observed while surveying. This is a typical cross-section where the two floodplains are at differing heights due to apparently natural causes and the width/depth ratio is high.

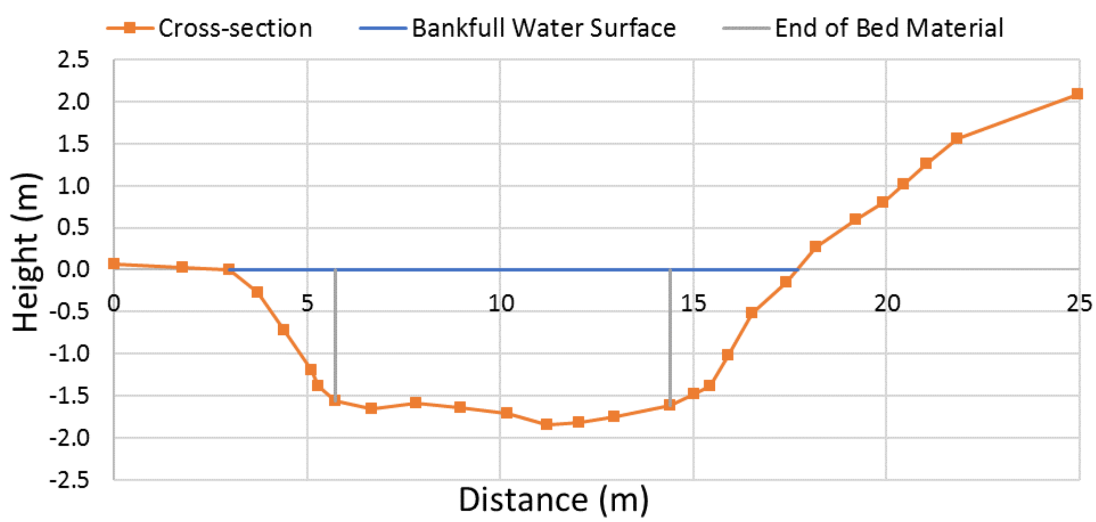

Figure 4.7. A graph depicting the river cross-section at site 8 looking downstream with a marked bankfull water surface line and ends of the channel material as observed while surveying. This is a typical cross-section where the two floodplains are at differing heights due to human interaction.

4.2.2 Surveys of Longitudinal River Profiles

The water surface slope was calculated for each reach (Table 4.2). The slopes ranged from 0.0008 for site 2 (Figure 4.8) to 0.0096 for site 16 (Figure 4.9). A typical longitudinal survey plot can be seen in Figure 4.10 of site 12, which shows some pool and riffle sequences for a reach about 400 meters long.

Table 4.2. A table reporting the starting and ending coordinates where water surface slope measurements were taken, as well as the method used and resulting slope values.

Site	Starting Coordinates	Ending Coordinates	Method	Slope
1	39°44'56.84"N, 75°46'9.60"W	39°44'49.84"N, 75°46'13.55"W	Longitudinal Survey	0.0037
2	39°43'47.49"N, 75°45'37.53"W	39°43'47.09"N, 75°45'42.72"W	Longitudinal Survey	0.0008
3	39°47'16.80"N, 75°49'10.98"W	39°47'11.00"N, 75°49'4.42"W	Longitudinal Survey	0.0039
4	39°45'47.48"N, 75°45'59.61"W	39°45'42.78"N, 75°46'2.82"W	Longitudinal Survey	0.0017
5	39°46'7.98"N, 75°45'48.24"W	39°46'3.72"N, 75°45'50.19"W	Longitudinal Survey	0.0029
6	39°47’22.17"N, 75°46’24.07"W	39°47’10.68"N, 75°46’24.28"W	Calculated from DEM	0.0045
8	39°48’9.07"N, 75°50’2.81"W	39°48’13.47"N, 75°49’46.80"W	Calculated from DEM	0.0031
9	39°48'54.50"N, 75°46'53.78"W	39°48'49.79"N, 75°47'0.19"W	Longitudinal Survey	0.0024
10	39°51'31.12"N, 75°46'59.80"W	39°51'17.11"N, 75°47'4.35"W	Supplied by Stroud Water Research Center	0.0059
11	39°51'45.50"N, 75°47'1.02"W	39°51'31.12"N, 75°46'59.80"W	Supplied by Stroud Water Research Center	0.0056
12	39°45'28.08"N, 75°47'1.31"W	39°45'18.60"N, 75°47'2.22"W	Longitudinal Survey	0.0046
14	39°47'15.01"N, 75°48'11.88"W	39°47'0.02"N, 75°48'12.80"W	Longitudinal Survey	0.0067
16	39°48'29.52"N, 75°45'15.40"W	39°48'25.61"N, 75°45'21.64"W	Longitudinal Survey	0.0096

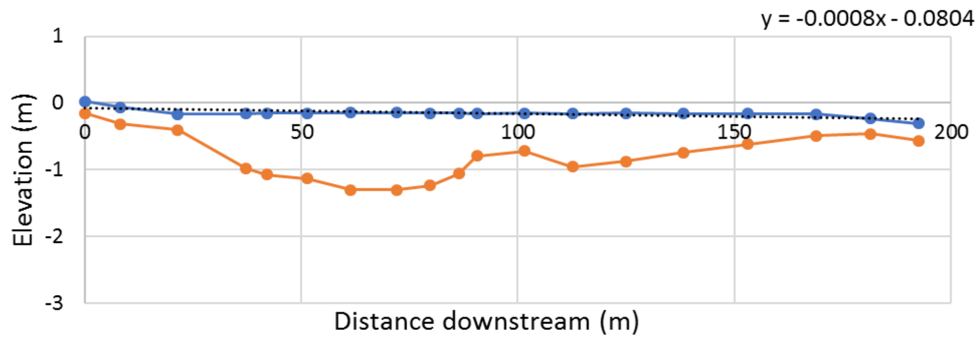

Figure 4.8. A graph depicting the longitudinal profile for Site 2 where the lowest slope was measured at 0.0008.

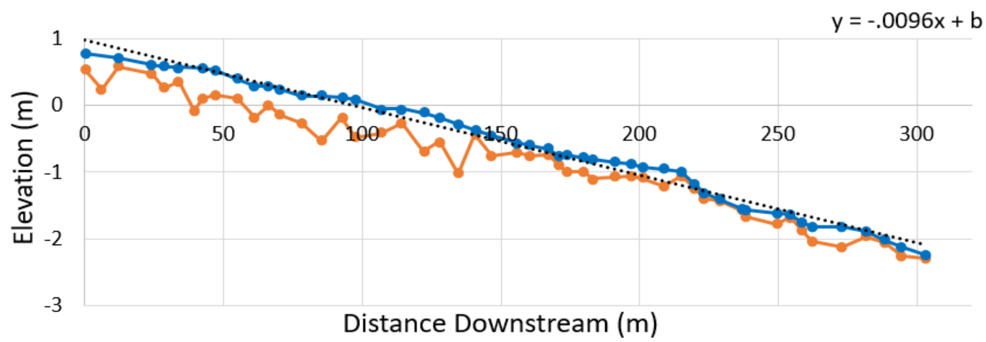

Figure 4.9. A graph depicting the longitudinal profile for Site 16 where the highest slope was measured at 0.0096.

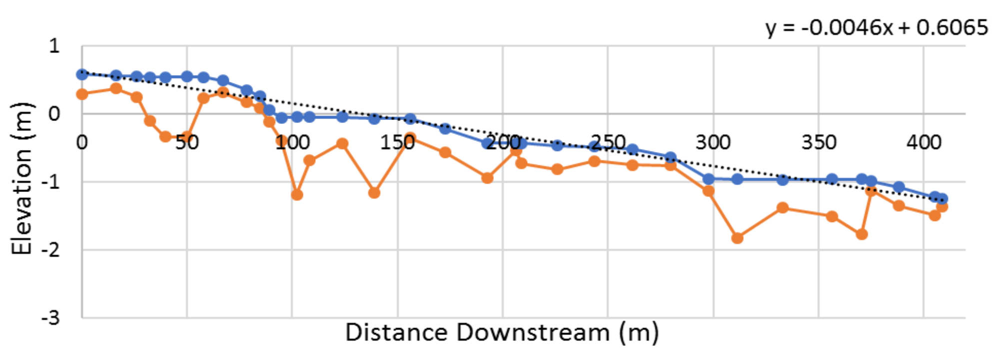

Figure 4.10. A graph depicting the longitudinal profile for site 12. Note the pool and riffle sequences and the slope of 0.0046.

4.3 Bank Erosion Rates

4.3.1 Historical Aerial Imagery Analysis

Bank erosion rates were quantified with aerial imagery techniques for eight sites (Table 4.3). Three sites (10us, 10mid, and 10ds) were digitized by Williamson (2013). Erosion rates quantified with this technique vary from 4.7 cm/yr for site 3 to 36.1 cm/yr for site 2 with a median value of 14.1 cm/yr. Site 10mid had the lowest area eroded per year at 3.96 m^2/yr and site 2 had the highest area eroded per year at 73.38 m^2/yr. The time over which lateral erosion rates were measured range from 3 years to 78 years. Care should be taken when comparing the rates to each other since rates could have slowed or quickened over time, which may or may not be considered in the range of years that each bank was measured. Figure 4.11 shows the digitization of bank lines and eroded areas for sites 2 and 5.

Table 4.3. A table reporting the year of each aerial image used, the time between the two years used, the total area eroded, the total area erosion rate, the length of the bank, and the reach averaged lateral erosion rate determined from historical aerial imagery.

Site	First Year	Last Year	Time between Images (yrs)	Area Eroded (m^2)	Area Eroded per Year (m^2/yr)	Length of Bank (m)	Erosion Rate (cm/yr)
2	1937	2015	78	5723.35	73.38	203.4	36.1
3	1937	2008	71	1004.48	14.15	70.3	20.1
5	1937	2015	78	1561.79	20.02	154.0	13.0
8	1937	2013	76	631.22	8.31	43.7	19.0
10us	1968	2010	42	187.73	4.47	45.3	9.9
10mid	1968	2010	42	166.40	3.96	32.8	12.1
10ds	1968	2010	42	200.87	4.78	31.3	15.3
16	2010	2013	3	14.33	4.78	17.2	27.8

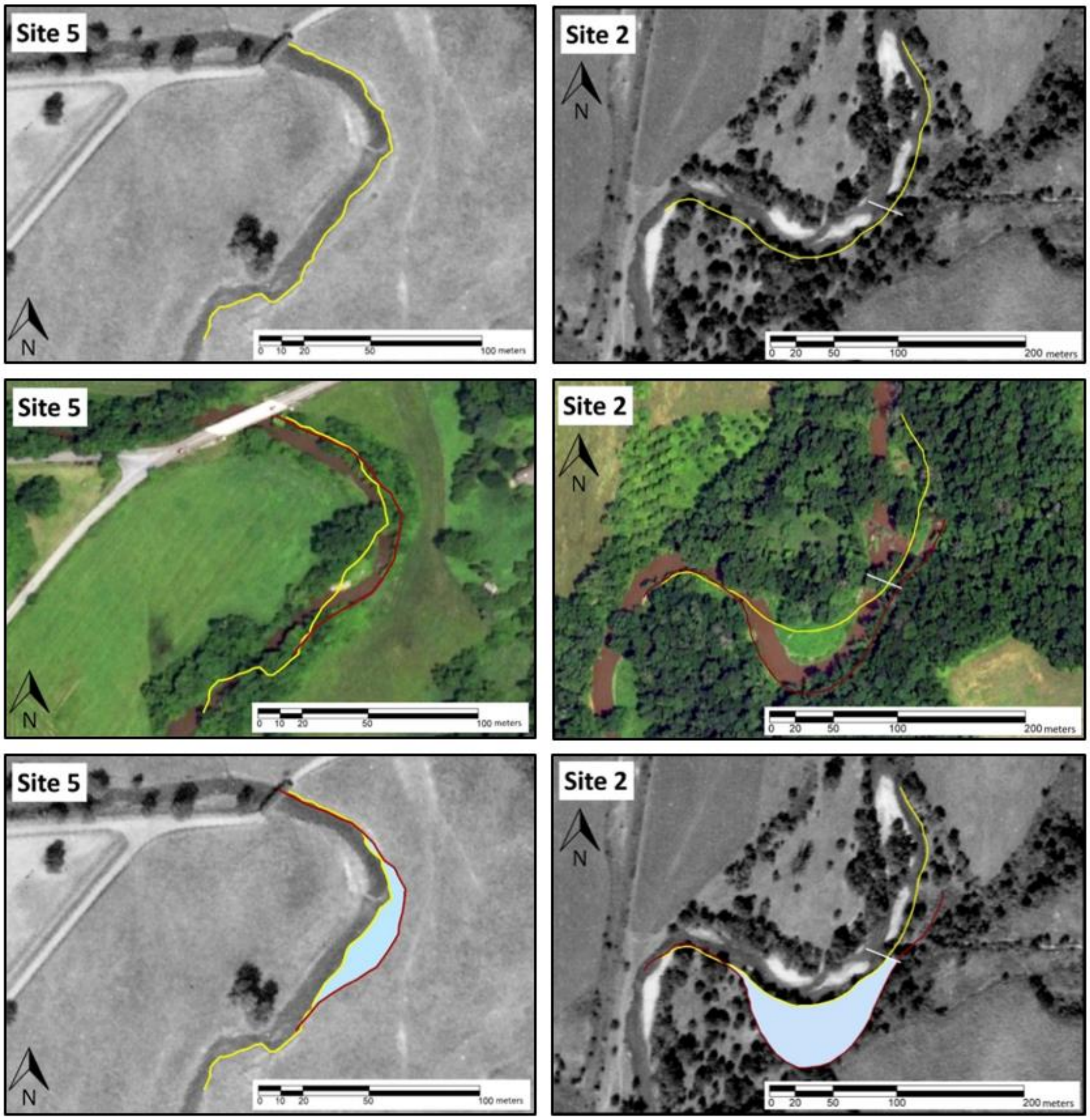

Figure 4.11. Aerial images with digitized bank lines from sites 5 and 2. The top images show digitized bank lines for 1937 (yellow), the middle maps show digitized bank lines for 1937 and 2015 (red), and the bottom maps show the area eroded between those two years.

4.3.2 Tree Root Dendrochronology

The locations of each sample are listed in Table 4.4, which also includes the type of tree and age at breast height. The year of exposure was identified for 28 root samples, while one root at site 6 was not considered due to the high uncertainty in identifying of the year of exposure. Pictures of the root samples that show the ring of initial exposure, and the indicators seen on each root sample are shown in Figure 4.13. At site 3, two root samples were taken, but identifying the year of exposure proved to be so difficult that aerial images were used instead. In both samples at site 3 there did not appear to be any indicators of exposure while in the unused sample at site 6, there were indicators, but counting the rings past the year of exposure proved difficult because of how close together the annual rings were.

Figure 4.12. An image depicting tree cores used to find the age at breast height of each sampled tree.

Successful samples included four tree roots at each of sites 1, 4, 6, 12, and 14, and eight tree roots at site 9. Williamson (2013) collected only one root at each of sites 11us, 11mid, and 11ds. The successful samples showed time of exposure to be between two and fifteen years, with erosion rates at the sample sites varying from 2.6 cm/yr to 23.2 cm/yr. The data used to calculate erosion rates at each tree are shown in Table 4.4.

Table 4.4. A table reporting tree root samples with their corresponding species, age at standard breast height, sample coordinates, bank retreat distance, number of years since exposure, root growth after exposure, average bark width, and lateral erosion rate of the bank behind each sample.

Site	Root	Tree Species	Tree Age at Breast Height (yr)	Coordinates of Sampled Tree	Bank Retreat Distance (cm)	Years since Exposure (yr)	Growth After Exposure (cm)	Bark Width (cm)	Erosion Rate at Sample (cm/yr)
1	test	black walnut	30+	39.74857392*N, 75.76985703*W	23.7	4	1.04	0.28	5.7
1	1	black walnut	42	39.74888999*N, 75.76970425*W	9.4	2	0.45	0.12	4.5
1	2	black walnut	20+	39.74841473*N, 75.76992533*W	39.5	3	0.73	0.23	13.0
1	3	white ash	45+	39.74885265*N, 75.76912609*W	6.9	2	0.29	0.24	3.4
4	1	black walnut	51+	39.76205824*N, 75.76744932*W	62.5	11	0.37	0.52	5.7
4	2	black walnut	56	39.76227445*N, 75.76738993*W	13.0	2	0.89	0.48	6.3
4	3	sycamore	47+	39.76228386*N, 75.76739824*W	88.5	7	1.48	0.07	12.4
4	4	mockernut hickory	48	39*45.751'N, 75*47.036'W	26.5	4	1.37	0.36	6.4
6	1	american elm	21	39.78640981*N, 75.77347599*W	9.9	3	0.67	0.04	3.1
6	2	oak	68	39.78646008*N, 75.77339378*W	31.9	4	0.22	0.46	8.0
6	3	oak	71+	39.78646929*N, 75.77339658*W	30.4	5	0.46	0.30	6.0
6	4a	beech	123	39.78652071*N, 75.77320345*W	48.2	7	1.07	0.12	6.7
9	A1	american wild crab apple	-	39*48.846'N, 75*46.979'W	17.5	3	0.37	0.20	5.8
9	B2	black walnut	48	39*48.846'N, 75*46.979'W	76.5	7	0.35	0.39	10.9
9	B3	black walnut	48	39*48.846'N, 75*46.979'W	154.0	11	0.93	0.23	13.9
9	C1	black walnut	29	39*48.858'N, 75*46.968'W	88.5	7	0.43	0.48	12.7
9	C2	black walnut	29	39*48.858'N, 75*46.968'W	92.5	4	0.50	0.45	23.1
9	D1	black walnut	45+	39*48.854'N, 75*46.969'W	21.0	7	0.45	0.54	3.0
9	E2	black walnut	47	39*48.854'N, 75*46.969'W	68.5	15	0.81	0.48	4.5
9	E3	black walnut	47	39*48.854'N, 75*46.969'W	23.0	2	0.12	0.34	11.6
12	1	hickory	41+	39*45'25.51"N, 75*47'4.69"W	100.5	6	1.01	0.12	16.6
12	2	yellow poplar	59+	39*45'25.63"N, 75*47'3.79"W	21.0	8	0.91	0.40	2.6
12	3	hickory	-	39*45'25.73"N, 75*47'3.50"W	16.5	5	0.89	0.17	3.2
12	4	hickory	92+	39*45'26.31"N, 75*47'2.51"W	40.5	2	0.23	0.16	20.2
14	1	yellow poplar	71+	39*47.136'N, 75*48.182'W	36.5	3	0.08	0.30	12.2
14	2	yellow poplar	90	39*47.131'N, 75*48.170'W	129.3	8	0.30	0.70	16.2
14	3	beech	-	39*47.113'N, 75*48.151'W	101.0	15	0.91	0.09	6.7
14	4	red maple	95	39*47.114'N, 75*48.147'W	92.9	4	0.28	0.13	23.2

The primary source of error comes from identifying the year of exposure. For example, in tree 4 at site 12, discolorations due to potential scarring suggest a year of exposure many years ago, but changes in vessel size and ring widths point to exposure occurring just two years ago. In tree 3 at site 14, ring width changes suggest exposure 4 years ago, but vessel arrangement and uneven formation of annual rings indicate exposure 15 years ago.

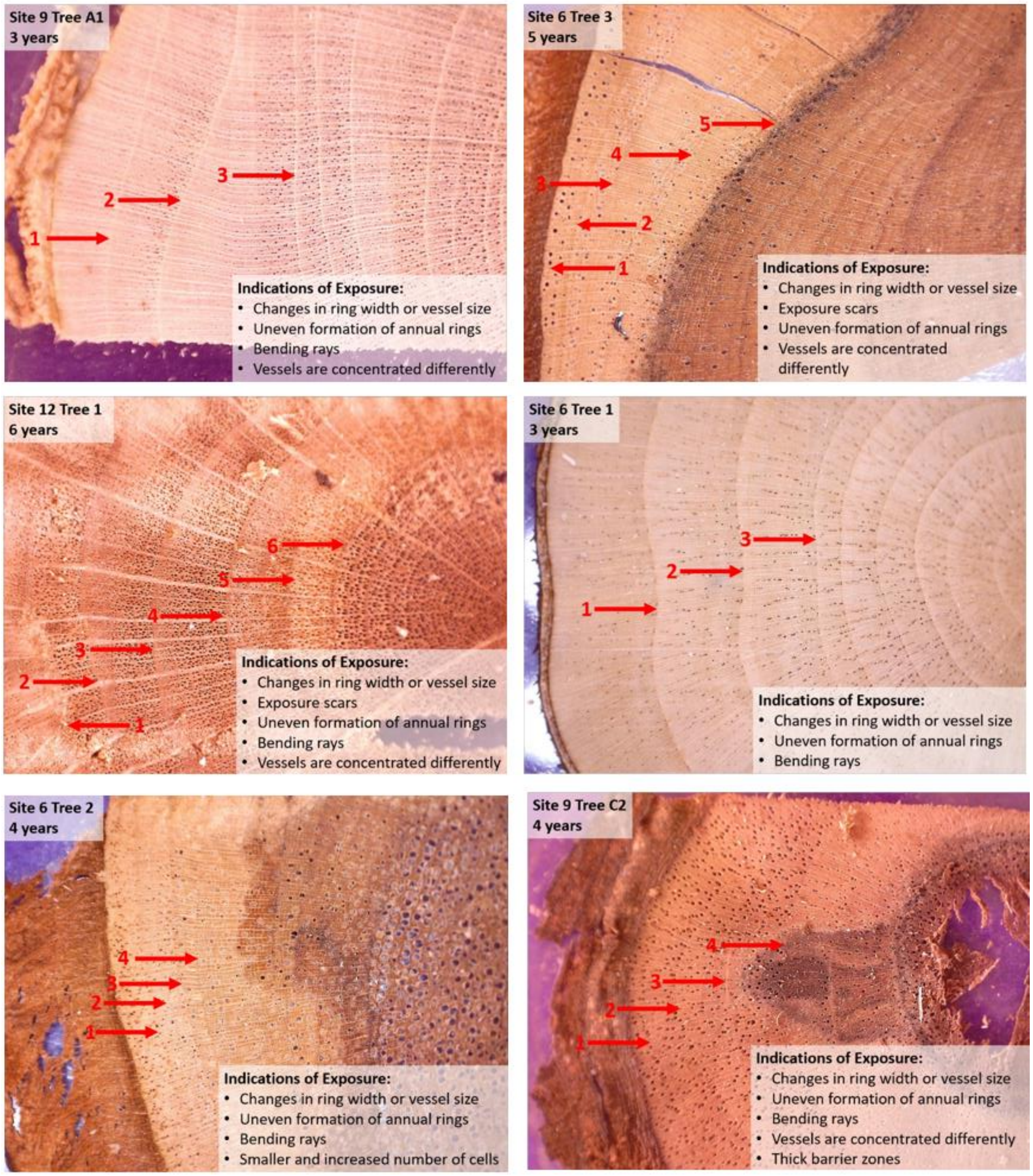

Figure 4.13. Images depicting root samples from sites 6, 9, and 12 under a microscope. Rings are marked pointing to rings that grew after exposure and indicators of exposure are listed.

4.3.3 Bank Height

The first order stream at site 16 had the shortest average bank height of 0.59 meters while site 5 had the tallest average bank height of 2.70 meters (Table 4.5). According to calculations of standard deviation the banks with the most height variation were sites 5 and 12, and those with the least were sites 10mid, 11us, and 16. On average the bank height increased with stream order: first and second order streams have banks between 0.59 meters and 1.58 meters tall, third and fourth order streams have banks between 1.40 meters and 2.70 meters tall.

Table 4.5. A table indicating the reach averaged bank height and corresponding standard deviation.

Site	Average Bank Height (m)	Standard Deviation (m)
1	2.22	0.36
2	1.74	0.31
3	1.14	0.19
4	1.50	0.17
5	2.70	0.56
6	1.88	0.16
8	1.58	0.22
9	1.40	0.36
10us	1.12	0.15
10mid	0.94	0.10
10ds	0.94	0.15
11us	0.97	0.10
11mid	1.36	0.49
11ds	0.95	0.23
12	2.47	0.51
14	1.34	0.32
16	0.59	0.10

4.3.4 Bulk Density

Bulk density was measured at all sites, with a single measurement used for site 10us, 10mid, and 10ds, and a single measurement used for site 11us, 11mid, and 11ds because of the proximity and similarity of the banks (Table 4.6). Measurements ranged between 1.02 g/cm^3 for site 6 and 1.48 g/cm^3 for site 12 with an average of 1.31 g/cm^3 and standard deviation of 0.12 g/cm^3. Only two samples were taken at site 6 because most of the bank was made up of gravels which proved difficult to sample. If results from site 6 are ignored, the next lowest bulk density is 1.21 g/cm^3 for site 16. On average, bulk density increases as you move down the bank face, but measurements are generally low for the finest sediment grain sizes.

Table 4.6. A table reporting the number of bulk density samples taken at each bank, the vertically averaged bulk density, and corresponding standard deviation.

Site	Number of Samples	Bulk Density (g/cm^3)	Standard Deviation (g/cm^3)
1	9	1.23	0.02
2	5	1.28	0.02
3	8	1.37	0.04
4	8	1.32	0.02
5	10	1.43	0.03
6	2	1.02	0.01
8	5	1.25	0.01
9	6	1.33	0.04
10	5	1.46	0.00
11	7	1.33	0.06
12	8	1.48	0.03
14	10	1.36	0.04
16	7	1.21	0.03

4.3.5 Mass Erosion Rates

The mass eroded per year was calculated at each bank (Table 4.7). The highest mass eroded per year was at site 2 with 163,705 kg/yr and a standard deviation of 29,415 kg/yr. The lowest mass eroded per year was at site 11us with 856 kg/yr and a standard deviation of 99 kg/yr. Standard deviations calculated for those sites where tree roots were used are highly over estimated due to methods of determining the bank averaged lateral erosion rate. To find a weighted average standard deviation, one must

Table 4.7. A table reporting the reach averaged lateral erosion rate, eroding bank length, total reach area erosion rate, reach averaged bank height, vertically averaged bulk density, total mass erosion rate, and corresponding standard deviation when calculated using the standard deviation of bulk density and bank height and also the standard deviation when considering the standard deviation calculated from the dendrochronology method as well.

Site	Erosion rate (cm/yr)	Bank Length (m)	Erosion Rate (m^2/yr)	Bank Height (m)	S.D. Bank Height (m)	Bulk Density (g/cm^3)	S.D. Bulk Density (g/cm3)	Erosion Rate (kg/yr)	S.D. Erosion Rate (kg/yr) due to bulk density and bank height	S. D. Erosion Rate (kg/yr) due to bulk density, bank height, and tree root method
1	6.2	97.0	5.970	2.22	0.36	1.23	0.02	16331	2671	13778
2	36.1	203.4	73.376	1.74	0.31	1.28	0.02	163705	29415	29415
3	20.1	70.3	14.130	1.14	0.19	1.37	0.04	22030	3677	3677
4	5.8	104.6	6.085	1.50	0.17	1.32	0.02	12080	1338	10705
5	13.0	154.0	20.023	2.70	0.56	1.43	0.03	77366	16173	16173
6	4.9	39.1	1.930	1.88	0.16	1.02	0.01	3697	309	3233
8	19.0	43.7	8.305	1.58	0.22	1.25	0.01	16371	2288	2288
9	9.8	62.0	6.091	1.40	0.36	1.33	0.04	11350	2920	9781
10us	9.9	45.3	4.467	1.12	0.15	1.46	0.00	7311	1004	1004
10mid	12.1	32.8	3.962	0.94	0.10	1.46	0.00	5443	596	596
10ds	15.3	31.3	4.783	0.94	0.15	1.46	0.00	6585	1061	1061
11us	2.2	30.0	0.667	0.97	0.10	1.33	0.06	856	99	99
11mid	1.4	48.3	0.676	1.36	0.49	1.33	0.06	1226	444	444
11ds	4.2	36.1	1.528	0.95	0.23	1.33	0.06	1929	475	475
12	9.1	82.8	7.556	2.47	0.51	1.48	0.03	27611	5731	24506
14	12.1	86.0	10.372	1.34	0.32	1.36	0.04	18874	4604	16714
16	27.8	17.2	4.775	0.59	0.10	1.21	0.03	3420	607	607

assume that the erosion rates at each of the root samples should be about the same, but this is not the case in nature. Banks are expected to erode more at varying places around a meander bend. Unfortunately, there is no standard method for determining error with these type of conditions, so standard deviations are wildly over estimated. This is in contrast to the standard deviation for those sites at which aerial imagery analysis was conducted. No error was assumed when calculations were made, though there may have been errors when georeferencing and digitizing bank lines. For these sites standard deviations are underestimated. For sites 11us, 11mid, and 11ds, though tree root dendrochronology was used, a standard deviation for bank erosion rate was not calculated since only one root sample was collected (Williamson, 2013).

4.4 Riparian Vegetation

Results for riparian tree density are reported in Table 4.8. The number of trees at each site ranged from zero trees at site 10us, 10mid, 10ds, and 16, to sixty trees at site 12. Of the sites with trees, about 30% of the trees can be considered large trees, trees with breast height cross-sectional areas greater than 1000 cm^2. Site 8 had no large trees and sites 6, 9, and 11mid had more than 50% large trees. There is a positive linear correlation ($R^2 = 0.73$) between the number of trees and large trees. The percentage of trees by area ranged from 0% for tree-less sites to 1.79% for site 12. The percentage of large trees by area ranged from 0% for site 8 and the four tree-less sites to 1.56% for site 12. The tree density by number ranged from 0 trees/m^2 for the tree-less sites to 0.15 trees/m^2 for site 12. The large tree density by number ranged from 0 trees/m^2 for site 8 and the tree-less sites to 0.06 trees/m^2 for site 12.

Table 4.8. A table reporting data collected for riparian vegetation. This includes the area five meters bank from the eroding banks, the amount of trees measured at each site, the amount of large trees, total cross-sectional areas of all tree trunks and just large tree trunks, the percent trees and large trees by area, and the tree density and large tree density.

Site	Area 5m back from eroding bank (m^2)	Amount of trees	Amount of large trees	Total cross-sectional areas of trunks (m^2)	Total cross-sectional area of large trunks (m^2)	Percent trees by area (%)	Percent large trees by area (%)	Tree density (trees/m^2)	Large tree density (large trees/m^2)
1	500	38	8	2.88	1.61	0.58	0.32	0.076	0.016
2	863	23	6	1.94	1.20	0.22	0.14	0.027	0.007
3	353	30	1	0.59	0.17	0.17	0.05	0.085	0.003
4	501	27	8	1.93	1.17	0.39	0.23	0.054	0.016
5	569	9	1	0.71	0.41	0.13	0.07	0.016	0.002
6	197	11	6	1.42	1.31	0.72	0.67	0.056	0.030
8	219	6	0	0.20	0.00	0.09	0.00	0.027	0.000
9	315	13	7	2.07	1.84	0.66	0.58	0.041	0.022
10us	261	0	0	0.00	0.00	0.00	0.00	0.000	0.000
10mid	173	0	0	0.00	0.00	0.00	0.00	0.000	0.000
10ds	176	0	0	0.00	0.00	0.00	0.00	0.000	0.000
11us	145	18	3	1.00	0.38	0.69	0.26	0.124	0.021
11mid	276	7	4	0.90	0.76	0.33	0.27	0.025	0.014
11ds	206	9	3	2.85	2.59	1.38	1.26	0.044	0.015
12	412	60	23	7.39	6.42	1.79	1.56	0.146	0.056
14	426	23	11	4.96	3.93	1.16	0.92	0.054	0.026
16	132	0	0	0.00	0.00	0.00	0.00	0.000	0.000

4.5 Near-bank Velocity

Model input includes hydraulic radius, bankfull channel width, water discharge, bed slope, a friction factor, D_{90}, and the total length of the reach to be modeled. The model produced images like those shown in Figures 4.13 and 4.14 of a velocity color map as water moves downstream. The calculated water discharge varies between 0.74 m^3/s for site 16 and 118.21 m^3/s for site 1 (Table 4.9). The calculated friction factors vary between 0.00645 for site 9 and 0.01704 for site 16. Values for D_{90} show a median of 0.14 meters and vary between .03 meters for site 16 and 0.46 meters at site 12. Site 6 had the fastest near-bank velocity at 4.18 m/s (Figure 4.14) and site 11us had the lowest at 1.07 m/s (Figure 4.15).

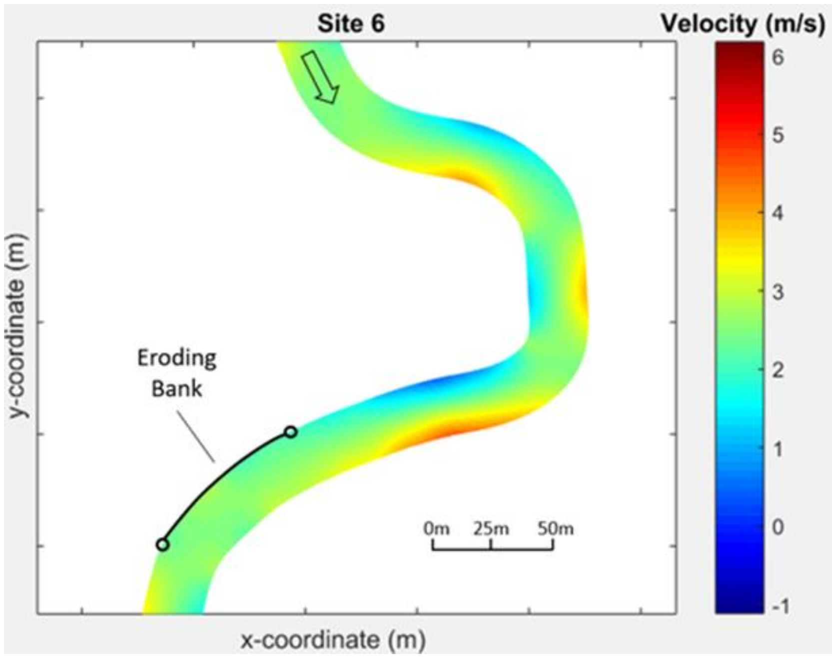

Figure 4.14. An image depicting a velocity map at site 6 including the labeled eroding bank. Note the high velocity values along the eroding bank.

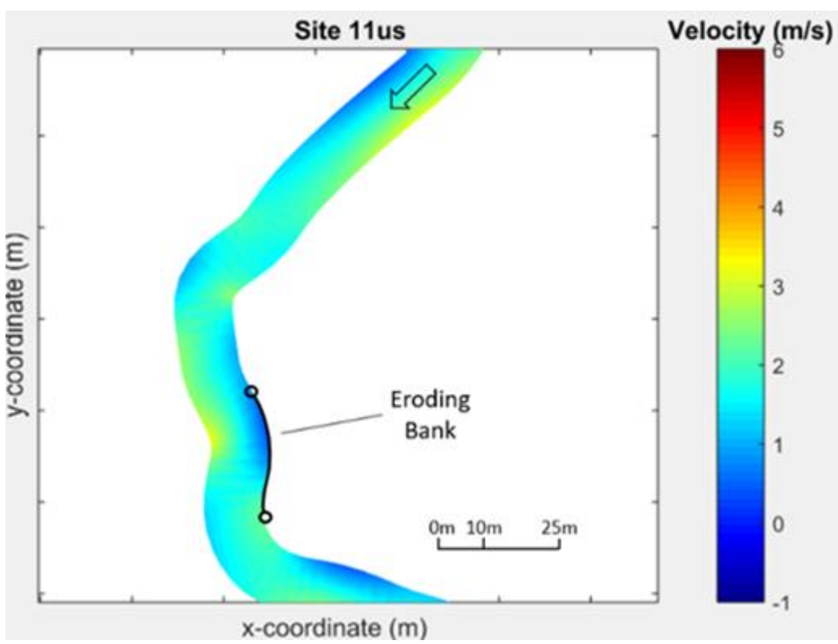

Figure 4.15. An image depicting a velocity map at site 11us including the labeled eroding bank. Note the low velocity values along the eroding bank.

Table 4.9. A table of near-bank velocity results and input variables to run the Matlab velocity model including hydraulic radius, bankfull width, water discharge, slope, a friction factor, D_{90}, and the length of the reach.

Site	Hydraulic Radius (m)	Bankfull channel width (m)	Water discharge (m^3/s)	Slope	Friction factor	D_{90} (m)	Length of modeled reach (m)	Near-bank velocity (m/s)
1	1.87	22.47	118.21	0.0037	0.00857	0.32	2363.1	2.79
2	1.34	36.03	56.34	0.0008	0.00771	0.12	3480.5	1.10
3	0.95	15.19	26.90	0.0039	0.0105	0.15	2277.1	2.33
4	1.16	21.03	31.41	0.0017	0.0117	0.31	2772.3	1.31
5	1.45	21.06	63.47	0.0029	0.00948	0.26	2082.6	2.80
6	1.49	26.49	99.84	0.0045	0.0103	0.35	3767.1	4.18
8	1.26	14.71	39.42	0.0031	0.00846	0.14	2582.6	2.05
9	1.43	14.57	47.56	0.0024	0.00645	0.08	1869.9	2.72
10us	0.58	9.09	8.90	0.0059	0.0118	0.08	1183.2	2.16
10mid	0.58	9.09	8.90	0.0059	0.0118	0.08	1183.2	1.40
10ds	0.58	9.09	8.90	0.0059	0.0118	0.08	1183.2	2.36
11us	0.69	12.75	15.85	0.0056	0.0117	0.11	803.5	1.07
11mid	0.69	12.75	15.85	0.0056	0.0117	0.11	803.5	2.25
11ds	0.69	12.75	15.85	0.0056	0.0117	0.11	803.5	1.48
12	1.28	30.43	83.86	0.0046	0.0125	0.46	2950.4	2.11
14	1.43	22.45	94.45	0.0067	0.0109	0.38	2637.9	3.52
16	0.19	3.80	0.74	0.0096	0.0170	0.03	597.1	1.69

4.6 Bank Material Strength

An average bank material strength was determined at each site with a single measurement used for site 10us, 10mid, and 10ds, and a single measurement used for site 11us, 11mid, and 11ds because the banks were relatively uniform (Table 4.10). Bank strength was highest at site 12 with a value of 49.0 kPa and standard deviation of 14.4, and was lowest at sites 11us, 11mid, and 11ds with a value of 21.5 kPa and standard deviation of 6.6 kPa. The most variation was seen at site 5, where values ranged from 17 kPa to 78 kPa resulting in an average value of 43.5 kPa and standard deviation of 21.4 kPa. Most banks' average values fell between 23 kPa and 33 kPa.

The average bank strength is correlated (R^2 = .248) with average bank bulk density (Figure 4.16). This means that more tightly packed material is stronger and that banks with more clay layers, and therefore higher porosity, will have a lower bulk density, and therefore a lower bank strength.

Table 4.10. A table reporting the number of bank strength measurements taken, the reach averaged bank strength, and corresponding standard deviation.

Site	Number of Measure-ments	Bank Strength (kPa)	Standard Deviation (kPa)
1	10	25.5	7.9
2	10	28.7	9.2
3	10	27.0	7.7
4	10	22.9	8.3
5	10	43.5	21.4
6	10	23.2	13.2
8	12	26.5	13.3
9	10	27.9	3.8
10	10	29.9	4.4
11	10	21.5	6.6
12	10	49.0	14.4
14	10	32.3	16.9
16	6	31.8	9.7

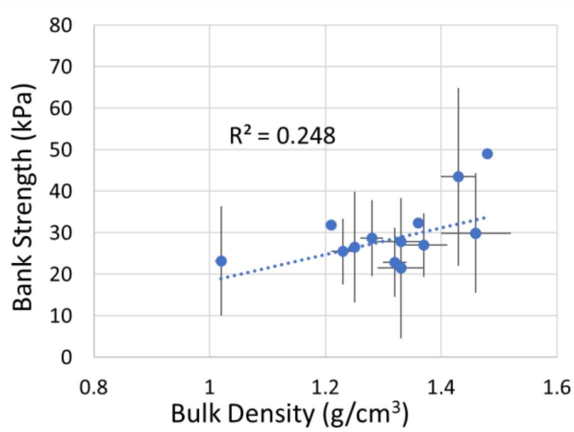

Figure 4.16. A plot of the reach averaged bulk density versus the reach averaged bank strength showing a positive correlation (R^2 = 0.248).

Chapter 5

DISCUSSION

5.1 Riparian Vegetation

Of the three main predicted controls to bank erosion that were tested, riparian vegetation seems to have the most direct influence. Lateral bank erosion rates were plotted against percent trees by area (Figure 5.1), percent large trees by area (Figure 5.2), tree density (Figure 5.3), and large tree density (Figure 5.4).

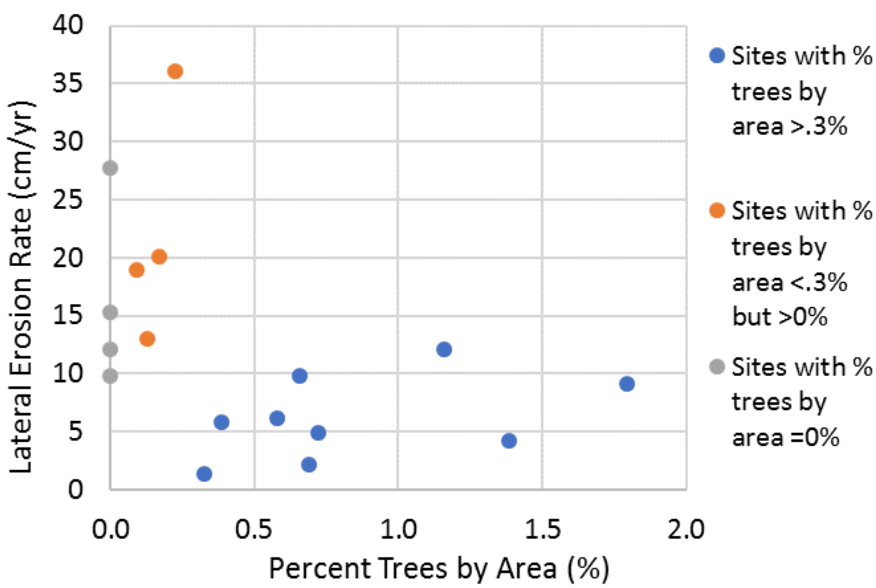

Figure 5.1. A plot of the percent trees by area versus lateral erosion rate. Note that for sites with a high percent of trees by area erosion rates fall below 12.5 cm/yr, but for sites with zero or a low percent trees by area erosion rates vary from 9.9 cm/yr to 36.1 cm/yr.

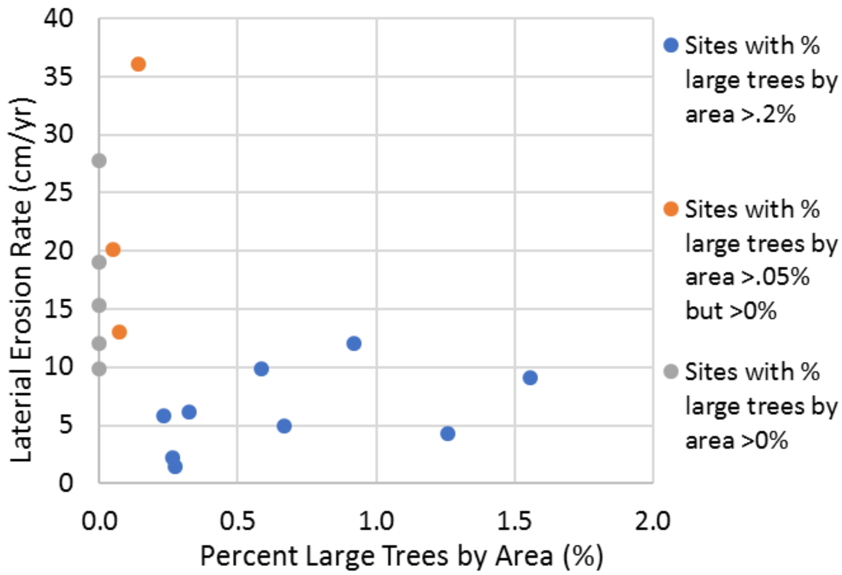

Figure 5.2. A plot of the percent of large trees by area versus lateral erosion rate. Note that for sites with a high percent of large trees by area erosion rates fall below 12.5 cm/yr, but for sites with zero or a low percent large trees by area erosion rates vary from 9.9 cm/yr to 36.1 cm/yr.

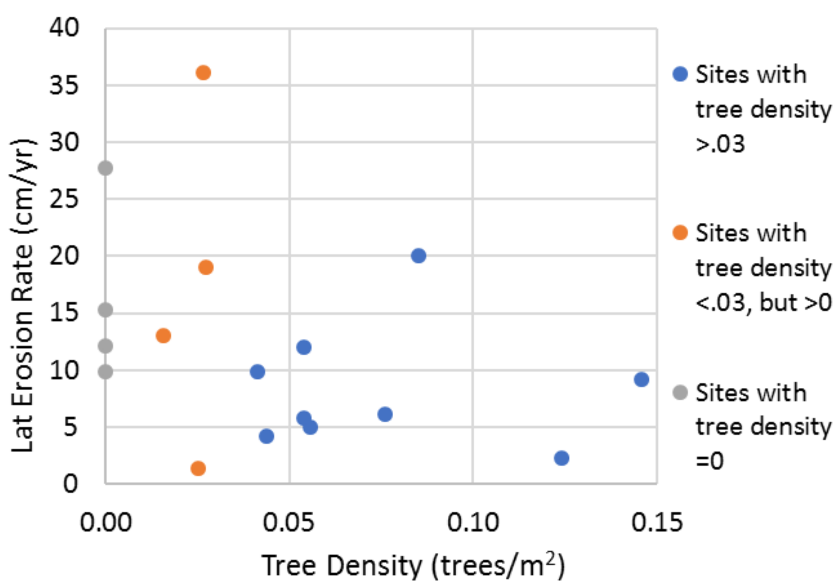

Figure 5.3. A plot of the tree density versus lateral erosion rate. Trends related to varying tree density are less apparent here.

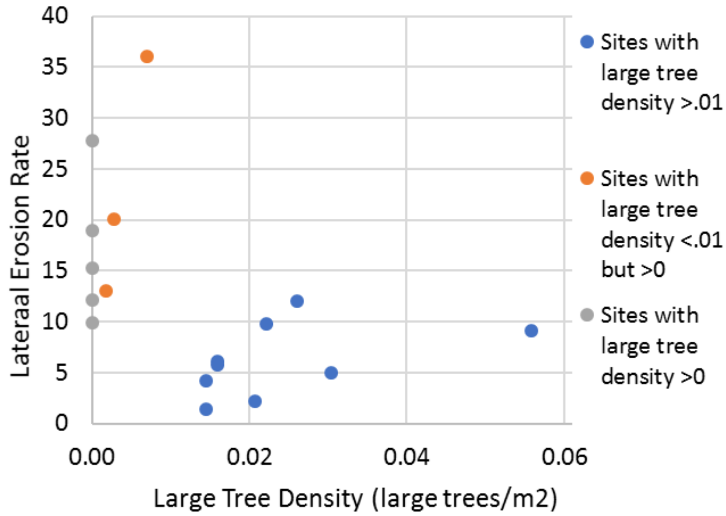

Figure 5.4. A plot of the large tree density versus lateral erosion rate. Note that for sites with a large tree density erosion rates fall below 12.5 cm/yr, but for sites with zero or a low large tree density erosion rates vary from 9.9 cm/yr to 36.1 cm/yr.

Figure 5.1 of percent trees by area versus erosion rate shows that those sites with more than 0.3% trees by area all have erosion rates under 12.5 cm/yr. For banks with less than 0.3% trees by area erosion rates vary from 9.9 cm/yr to 36.1 cm/yr. It appears that trees growing in the riparian zone have some control over the amount of erosion that occurs and in places where trees do not dominate, erosion rates vary greatly, potentially dependent on other factors. This same pattern is seen when looking at the percent of large trees by area (Figure 5.2). For sites with a percent of large trees by area greater than 0.2% the erosion rate again stays under 12.5 cm/yr. For those sites with less than 0.2% large trees by area, erosion rates vary again from 9.9 cm/yr to 37.1 cm/yr. This makes sense since it can be shown that the number of large trees at a site increases with an increase in the number of trees in general. This same trend applies for large tree density with erosion rates below 12.5 cm/yr for all sites with a large tree density greater than 0.01 large trees/m^2, and between 9.9 cm/yr and 36.1 cm/yr for sites with a large tree density less than this (Figure 5.4). The pattern is less defined when looking at tree density for all trees (Figure 5.3). Past studies on the effects of riparian vegetation on erosion rates have shown similar trends. For example, Pizzuto and Meckelnburg (1989) found that larger trees right along the edge of the bank dramatically decrease erosion rates, and Wynn et. al (2004) showed that an increase in root size and density, which vary with the type and size of vegetation, can decrease erosion rates.

5.2 Near-bank Velocity

There does not seem to be any correlation between near-bank velocity and lateral erosion rates (Figure 5.5). The data yield an R^2 value of 0.05 and p-value of 0.37. Another plot in Figure 5.6 shows near-bank velocity versus lateral erosion rate but only for those eight banks that are not dominated by riparian trees. This produced a R^2 value of 0.371 but a p-value of 0.11. Based on these results it doesn't seem that near-bank velocity alone has much influence; in fact, the values are negatively correlated which is not expected. Other studies have been successful in showing a positive correlation between near-bank velocity and bank erosion rates since bank erosion processes, especially those at the toe of the bank, are fluvially controlled.

Potential inaccuracies within the data may be due to problems within the model. A potential inaccuracy of near-bank velocity at Site 1 should be considered because of trouble applying the model to this site. The upstream end of the eroding bank at site 1 is about 40 meters downstream of the confluence of the East and West/Middle branch of the White Clay Creek. The model used is not capable of factoring in more than one branch of a stream. The model was run and data was

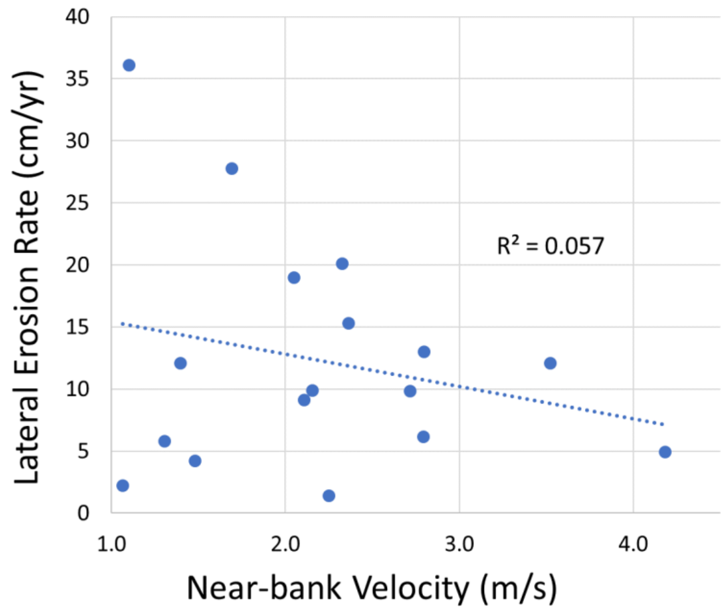

Figure 5.5. A plot depicting near-bank velocity versus lateral erosion rate. Note the poor trend (R^2 = 0.057, p = 0.37).

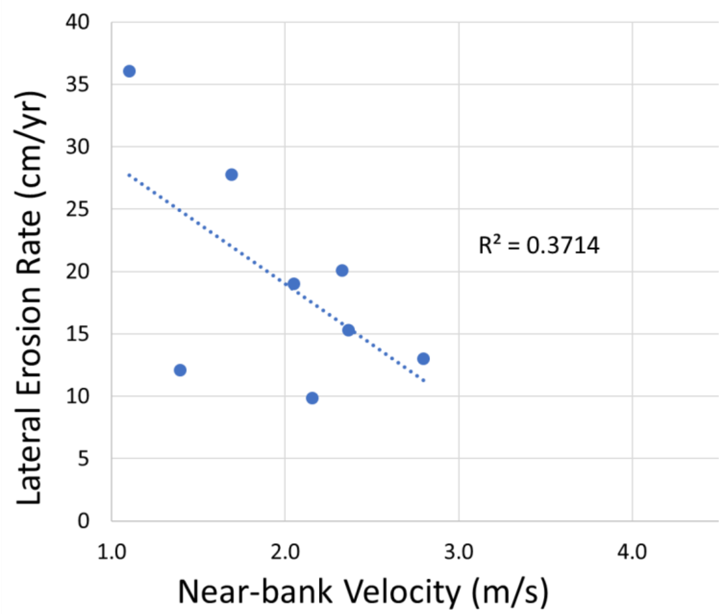

Figure 5.6. A plot depicting near-bank velocity versus lateral erosion rate for only those sites not dominated by riparian trees. Note the poor trend (R^2 = 0.371, p = 0.11).

collected by ignoring each branch one at a time. When the influence of the East branch is ignored, the near-bank velocity along the eroding bank is 2.47 m/s and when the influence of the West/Middle branch is ignored the near-bank velocity is 2.22 m/s. The near-bank velocity reported in Table 4.9 is 2.79 m/s which is the value received when a channel centerline is drawn up to the confluence and then continued out in a straight line. Also the model is not supposed to produce negative velocities anywhere within the given stream reaches. Negative modeled velocities do appear though in up and downstream portions of the modeled stream reaches (Figure 5.7). Values of near-bank velocity at the eroding bank sites do not show any negative velocities though.

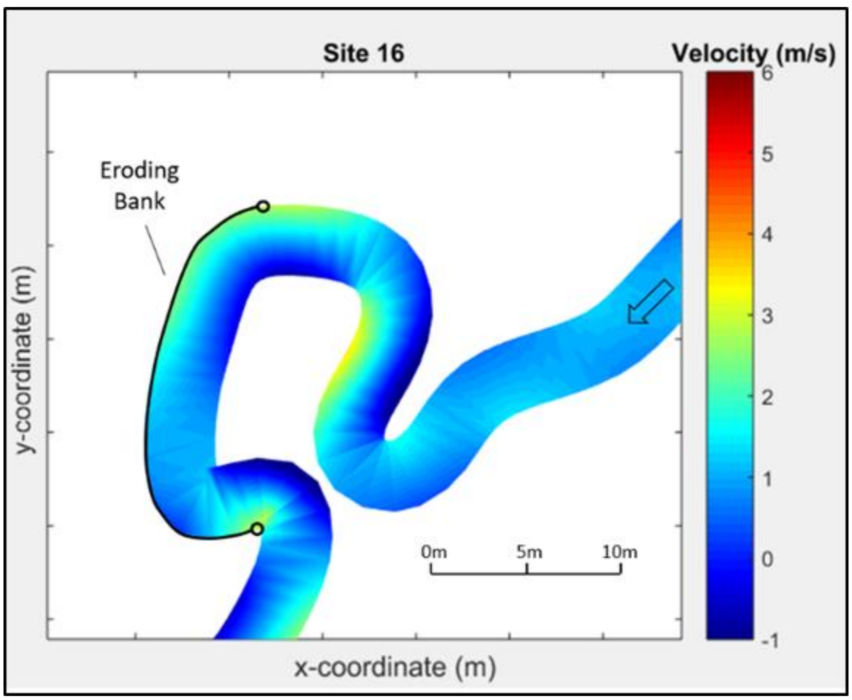

Figure 5.7. An image showing the Matlab output at site 16 including a velocity map of the entire reach and the labeled eroding bank. Note the negative velocity values within the reach, but not along the eroding bank.

The lack of correlation could be caused by the characteristics of the bank sediment as well. For banks of homogeneous sediment material, near-bank velocity has been shown to have a great influence over erosion rates. It was shown that in stratified banks or those of homogeneous material, like the banks in this study, near-bank velocity seems to have a smaller influence compared to some other variables (Thorne and Tovey, 1981; Pizzuto and Meckelnburg, 1989; Pizzuto, 1984).

The lack of correlation here could also be due to the model's lack of consideration for riparian vegetation and the density of roots hanging over the banks. A study by Thorne and Furbish (1995) looked at the flow field in the stream along eroding banks covered by thick roots and hanging plants and then cleared the bank of vegetation and observed the flow field again. They found that for banks that lacked vegetation, the highest stream velocity was found much closer to the bank face on the outside edge of the meander, as well as further upstream on the bend, while thick vegetation along the eroding bank of a meander caused the flow pattern to be disrupted preventing high velocity flows from ever directly hitting the bank face. Since the near-bank velocity model has not considered this influence from vegetation, it is possible that the near-bank velocities reported may not be representative of what actually occurs directly adjacent to bank faces of varying vegetation densities.

5.3 Bank Material Strength

The sediment type within the basal layer of each eroding bank seems to have some influence over the rates of erosion. The common cycle of bank erosion includes fluvial scour of the toe of the bank, undermining, and eventually bank failure, so it is clear that for average flow conditions the layer of sediment with the most influence on erosion rates is the basal layer at and below the water level (Thorne and Tovey, 1981).

The eroding banks in this study can be divided into two groups based on the material in the base layer of the bank; one consisting of mostly mud and the other consisting of mostly sand or gravel. The average lateral erosion rate for the eight banks with a base layer of mostly mud is 17.0 cm/yr with a standard deviation of 9.6 cm/yr. For the nine banks with a base layer of mostly sand or gravel the average lateral erosion rate is 8.1 cm/yr with a standard deviation of 5.7 cm/yr. A two-sample t-test was performed and returned a t-value of 2.16 and a p-value of 0.05. A box plot shows the considerable difference in mean erosion rate between the two categories (Figure 5.8), although more data should be collected in order to further confirm or deny the validity of this trend.

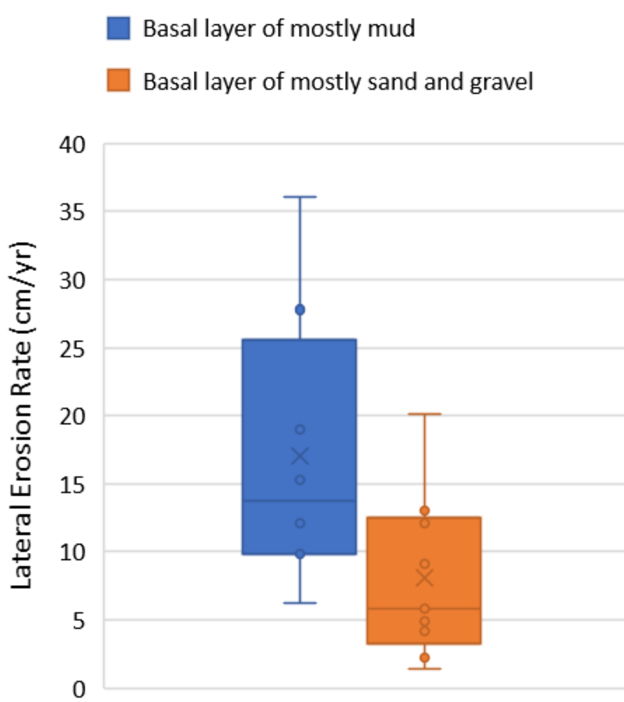

Figure 5.8. A box plot showing the reach averaged lateral erosion rates for banks with basal layers of mostly mud versus those of mostly sand and gravel.

There does not appear to be any correlation between bank strength and lateral bank erosion rates for these sites. Figure 5.9 shows a plot of the bank strength values averaged for the entire bank as well as for just the basal layer. Since riparian trees seem to have an influence, the same data were plotted again but only for those eight sites in which trees do not dominate the bank, but again there was a lack of any correlation (Figure 5.10).

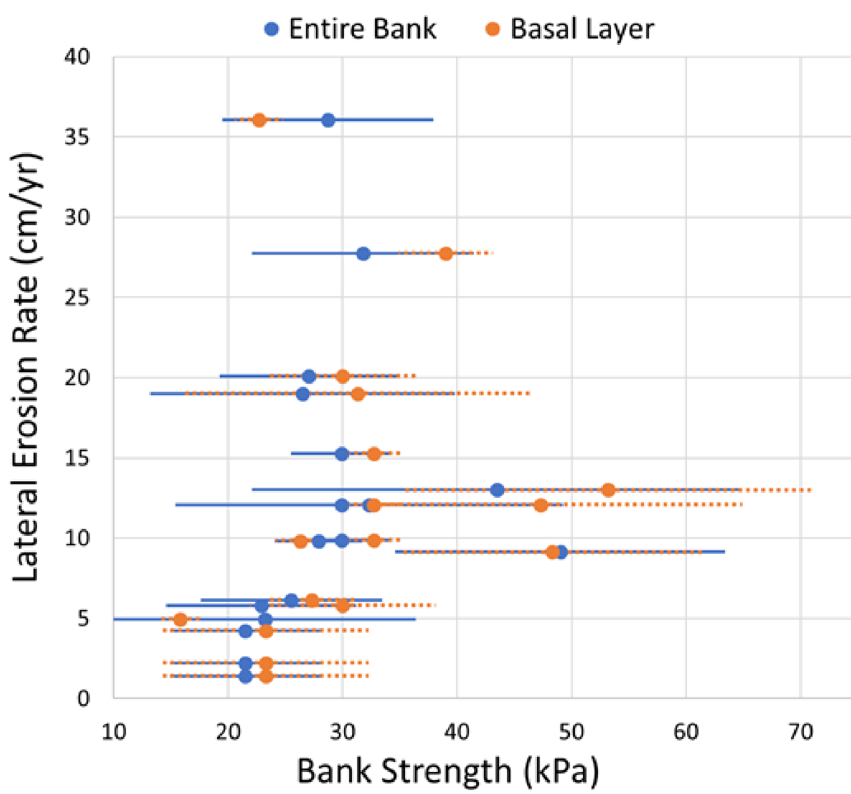

Figure 5.9. A graph of bank strength versus lateral erosion rate for the entire bank as well as for just the basal layer. Note the lack of any trend.

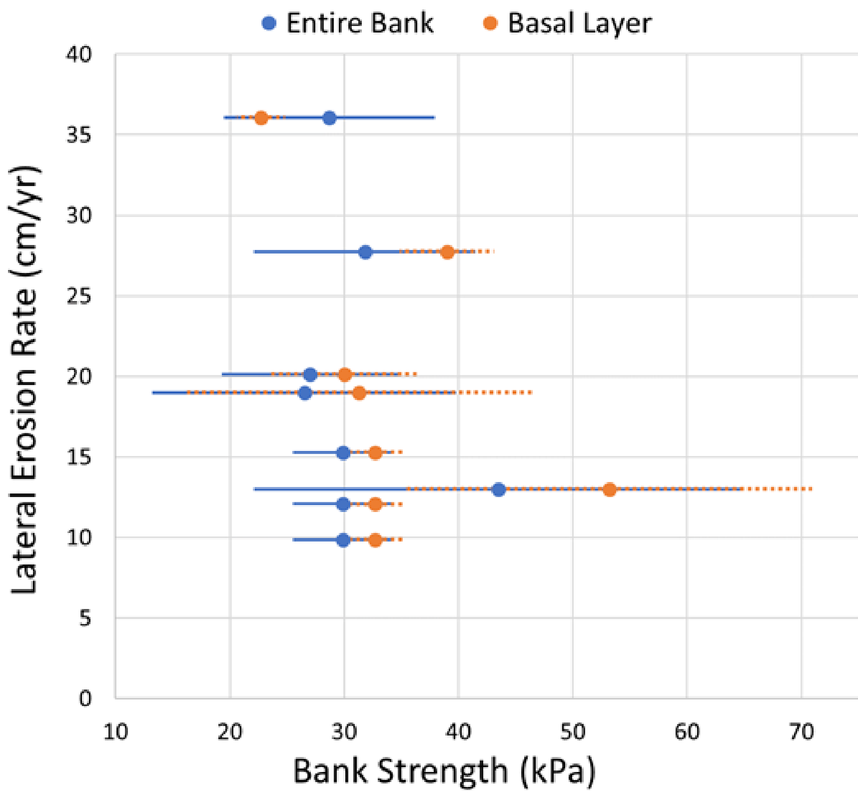

Figure 5.10. Graph of bank strength versus lateral erosion rate for the entire bank as well as for just the basal layer, only for those sites not dominated by trees. Note the lack of any trend.

It is important to note that bank strength can be influenced by other factors so these results are not entirely surprising. A study by Simon et al. (2000) states that seepage forces of water going into and out of the bank play a huge role in determining bank strength, due to the resulting changes in pore-water pressures. Since hydrological conditions can change rapidly, it is not enough to say that conditions were uniform site-to-site even though the sampling was completed within the same 20-day period. Also we do not know whether the bank at the time of sampling was acting as it "normally" does and how often "abnormal" conditions occur.

5.4 Freeze-thaw Cycles

The influence of freeze-thaw processes on erosion rates was not included in this study. Others have initiated studies to document these processes. It appears that freeze-thaw cycles may have a large impact on certain banks as needle-ice and other ice structures have been observed on many of the banks in this study (Figures 5.11, 5.12, and 5.13. This is not surprising as winter temperatures in this area often reach above and below the freezing point daily.

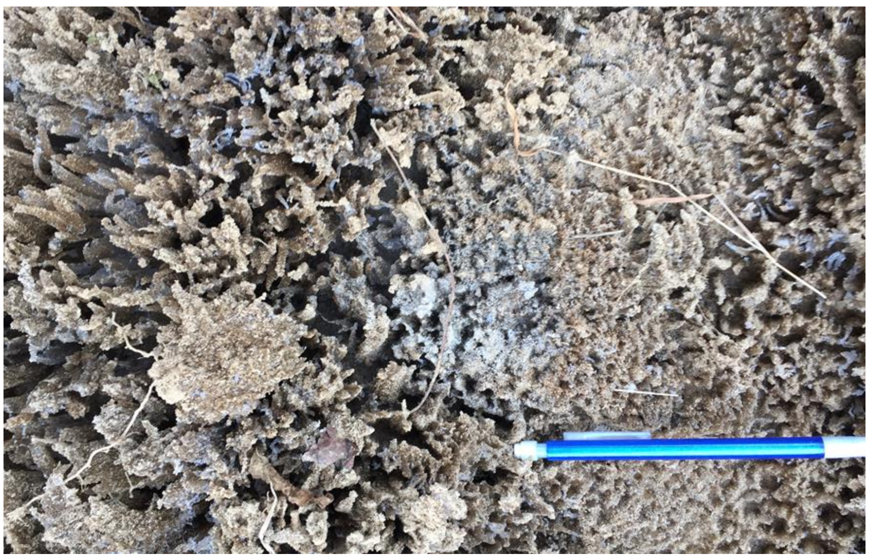

Figure 5.11. An image depicting needle-ice structures on the eroding bank at site 8.

Figure 5.12. An image depicting freeze-thaw structures on an eroding bank at site 16.

Figure 5.13. An image depicting freeze-thaw structures on the bank at site 11.

Chapter 6

CONCLUSIONS

In this study bank erosion rates were measured using tree root dendrochronology and historical aerial imagery analysis. Reach averaged lateral erosion rates varied from 1.4 cm/yr to 36.1 cm/yr. Bank eight and bulk density was determined in order to find erosion rate values in mass of eroded sediment per unit time. These ranged from 856 kg/yr to 163705 kg/yr. Measurements of controls of bank erosion including riparian vegetation, near-bank velocity, and bank strength, were determined. It appears that the amount and size of riparian trees is the primary control on bank erosion rates since sites dominated by riparian trees have lateral erosion rates less than 12.5 cm/yr, and other sites not dominated by riparian trees have erosion rates that vary from 9.9 cm/yr to 36.1 cm/yr. Near-bank velocity and bank strength both showed no correlation with lateral erosion rates, but bank descriptions show a significant difference in mean lateral erosion rates between those sites with a basal layer of mostly mud or mostly sand and gravel, of which the sites with basal layers of mostly sand and gravel have significantly lower lateral erosion rates. Data should be collected at more sites to better understand the controls on erosion rates and results of future freeze-thaw process studies should be considered as well.

REFERENCES

Allmendinger, N. E., Pizzuto, J. E., Potter, N., Johnson, T. E., & Hession, W. C. (2005). The influence of riparian vegetation on stream width, eastern Pennsylvania, USA. Bulletin of the Geological Society of America, 117(1–2), 229–243.

Bricker, O. P., Paces, T., Johnson, C. E., & Sverdrup, H. (1994). Weathering and Erosion Aspects of Small Catchment Research. Biogeochemistry of Small Catchments: A tool for Environmental Research.

Corona, C., Saez, J.L., Rovera, G., Stoffel, M., Astrade, L., Berger, F. (2011). High resolution, quantitative reconstruction of erosion rates based on anatomical changes in exposed roots at Draix, Alpes de Haute-Provence-critical review of existing approaches and independent quality control of results. Geomorphology 125 (3), 433-444.

Charlton, R. (2008). Fundamentals of Fluvial Geomorphology. New York, NY: Routledge.

Code of Ordinances County of New Castle, Delaware, Supplement 8 Update 2 § 40.10.126 RBA Design Standards (2016). https://www.municode.com/library/de/new_castle_county/codes/code_of_ordinances?nodeId=CH40UNDECO_ART10ENST_S40.10.126RBDEST

Cribb, C. (2017) Comparing high-resolution topographic survey methods for assessing geomorphic changes of point bars. (Master's Thesis).

Delaware Department of Natural Resources and Environmental Control, Division of Watershed Stewardship, University of Delaware's Water Resources Agency, White Clay Creek. Delaware Watersheds, http://delawarewatersheds.org/ piedmont/white-clay-creek/. (Accessed: 15th December 2016).

Duffield Associates: Soil, Water & the Environment (2017). White Clay Creek Stream Bank Restoration and Enhancement. http://duffnet.com/?page_id=521

Evans, B. M., Sheeder, S. A., Lehning, D. W. (2003). A special technique for estimating streambank erosion based on watershed characteristics. Journal of special Hydrology, 3(1).

Fayle, D. (1968). Radial growth in tree roots: distribution, timing, anatomy, Technical Report Number 9 Faculty of Forestry, University of Toronto, (183 pp.).

Gatto, L. W. (1995). Soil Freeze-Thaw Effects on Bank Erodibility and Stability. Prepared for the US Army Corps of Engineers: Office of the Chief of Engineers.

Gartner, H., Schweingruber, F.H., Dikau, R. (2001). Determination of erosion rates by analyzing structural changes in the growth pattern of exposed roots. Dendrochronologia, 19 (1), 81-91.

Hooke, J. M. (1979). Magnitude and Distribution of Rates of River Bank Erosion. Earth Surface Processes, 5, 143-157.

Jacobson, R. B., Coleman, D. J. (1986). Stratigraphy and recent evolution of Maryland Piedmont flood plains. American Journal of Science, 286, 617-637.

Kauffman, G. J., Wozniak, S. L., & Vonck, K. J. (2003). A Watershed Restoration Action Strategy (WRAS) for the Delaware Portion of the Christina Basin (United States of America, Christina Basin Clean Water Partnership, University of Delaware – Water Resources Agency). Newark, DE. http://www.wra.udel.edu/wpcontent/publications/Christina%20Basin%20Watershed%20Restoration%20Action%20Strategy%20Final%20Report.pdf

Lawler, D.M. (1988). Environmental limits of needle ice: a global survey. Arctic and Alpine Research, 20: 137-159.

Lawler, D. M. (1993). The measurement of river bank erosion and lateral change: a review. Earth Surface Process and Landforms, 18(9).

Leopold, L. B., Wolman, M. G. (1960). River meanders, Bulletin of the Geological Society of America, 71, 769-794.

Merritts, D., Walter, R., Rahnis, M., Hartranft, J., Cox, S., Gellis, A., Becker, S. (2011). Anthropocene streams and base-level controls from historic dams in the unglaciated mid-Atlantic region, USA. Philosophical Transactions of the Royal Society, 369, 976-1009.

Mogil, H. M. & Seaman, K. L. (2009). Weatherwise Magazine - The Climate and Weather of Delaware, Maryland, and Washington, D.C. Retrieved March 13, 2017, from http://www.weatherwise.org/ archives/ back%20issues/2009/july-august%202009/full-mogil.html

Narvaez, M., Homsey, A. White Clay Creek State of the Watershed Report: 2016. (University of Delaware Water Resource Agency, 2016). https://static1.squarespace.com/static/552801ede4b0f154af070737/t/56f0016d2b8dde509ab6f730/1458569584607/WhiteClayCreek_StateOfTheWatershedReport_Final_031416.pdf

Corrozi, M., Homsey, A., Kauffman, G., Farris, E., Seymor, M. White Clay Creek State of the Watershed Report. (University of Delaware Water Resources Agency, 2008). https://static1.squarespace.com/static/552801ede4b0f154af070737/t/56310c78e4b0dc92369baaff/1446055032924/White_Clay_Creek_final_070408_0.pdf

Natural Resources Conservation Service. Soil Quality Test Kit | NRCS Soils, Retrieved March 13, 2017, from https://www.nrcs.usda.gov/wps/portal/nrcs/detailfull/soils/health/assessment/?cid=nrcs142p2_053873

Nimick, D. A., Gammons, C. H., & Parker, S. R. (2011). Diel biogeochemical processes and their effect on the aqueous chemistry of streams. Chemical Geology, 283, 3-17.

Oberholtzer, W. (2011). Hydrologic and Hydraulic Processes and Connectivity In Altered Mid-Atlantic Riverine Systems. presented to Mid-Atlantic Stream Restoration Conference at Rocky Gap, Retrieved from https://www.fws.gov/chesapeakebay/masrc/MASRC%20PDFs/H_session_web/5_H_oberholtzer.pdf

Ottevanger, W., Blankaert, W. S., Uijttewaal, W. S. J., de Vriend, H. J. (2013). Meander dynamics: a reduced-order nonlinear model without curvature restictions for flow and bed morphology. Journal of Geophysical Research: Earth Surface, 118(2).

Perlman, H. (2014, March). Turbidity. In The USGS Water Science School. Retrieved from http://water.usgs.gov/edu/turbidity.html

Pizzuto, J. E. (1984). Bank erodibility of shallow sandbed streams. Earth Surface Processes and Landforms, 9, 113-124.

Pizzuto, J. E., Meckelnburg, T.S. (1989). Evaluation of a linear bank erosion equation. Water Resources Research 25: 1005-13

Pizzuto, J., O'Neal, M. (2009). Increased mid-twentieth century riverbank erosion rates related to the demise of mill dams, South River, Virginia. Geology, 37(1), 19-22.

Rhoades, E. L., O'Neal, M. A., Pizzuto, J. E. (2009). Quantifying bank erosion on the south river from 1937 to 2005, and its importance in assessing Hg contamination. Applied Geography, 29(1), 125-134.

Rosgen, D. L. (2001). A pracitical method of computing streambank erosion rate. Proceedings of the Seventh Federal Interagency Sedimentation Conference.

Simon, A., Curini, A., Darby, S. E., Langendoen, E. J. (2000). Bank and near-bank processes in an incised channel. Geomorphology, 35(3-4), 193-217.

Simon, A., Doyle, M., Kondolf, M., Shields Jr., F. D., Rhoads, B., McPhillips, M. (2007). Critical evaluation of how the Rosgen classification and associated “natural channel design” methods fail to integrate and quantify fluvial processes and channel response. Journal of the American Water Resources Association, 43(5).

Smith, N. D., Smith, D. G. (1984). William River: An outstanding example of channel widening and braiding caused by bed-load addition. Geology, 12, 78-82.

Stotts, S., O’Neal, M., Pizzuto, J., Hupp, C. (2014). Exposed tree root analysis as a dendrogeomorphic approach to estimating bank retreat at the South River, Virginia. Geomorphology, 223, 10-18.

Strahler, A. N. (1957). Quantitative analysis of watershed geomorphology. Transactions, American Geophysical Union, 38(6).

Thorne, C. R. (1981). Field measurements of rates of bank erosion and bank material strength. In Erosion and Sediment Transport Measurement, International Association of Hydrological Sciences Publication 133. IAHS Press: Wallingford; 503–512.

Thorne, C. R., Osman, A. M. (1988). Riverbank stability analysis II: applications. Journal of the Hydraulic Division, Proceedings of the American Society of Civil Engineers, 114: 151-172.

Thorne, C. R., Tovey, N. K. (1981). Stability of composite river banks. Earth Surface Processes and Landforms, 6(5), 469-484.

Thorne, S. D., Furbish, D. J. (1995). Influences of course bank roughness on flow within a sharply curved river bend, Geomorphology, 12, 241 – 257.

Turowski J.M., Hovius N., Wilson A. and Horng M.-J. (2008). Hydraulic geometry, river sediment and the definition of bedrock channels. Geomorphology, 99(1-4), 26-38.

United States Environmental Protection Agency (2007, November). Nonpoint Source Program Success Story: Delaware. Retrieved January 30, 2017, from https://www.epa.gov/sites/production/files/2015/11/documents/de_pikecreek.pdf

US Climate Data. Climate Newark - Delaware. Web. 14 Jan. 2017. http://www.usclimatedata.com/climate/newark/delaware/unitedstates/usde0043

United States Department of Agriculture, 1998. Field Book for Describing and Sampling Soils, Version 1.1., 212 p. https://www.nrcs.usda.gov/Internet/FSE_DOCUMENTS/nrcs142p2_052523.pdf

USGS 01478120 East Branch White Clay Creek at Avondale, PA. USGS Current Water Data for the Nation Available at: https://waterdata.usgs.gov/ usa/nwis/ uv?01478245. (Accessed: 10th February 2017).

USGS 01478245 White Clay Creek near Strickersville, PA. USGS Current Water Data for the Nation Available at: https://waterdata.usgs.gov/usa/nwis/ uv?01478245. (Accessed: 15th December 2016).

Wynn T. M., Mostaghimi, S., Burger, J. A., Harpold, A. A., Henderson, M. B., Henry, L. (2003). Variation in Root Density along Stream Banks. Journal of Environmental Quality, 33, 2030-2039.

Williamson, E. K. (2013). The effect of particle exchange on suspended sediment transport distances on the White Clay Creek, Pennsylvania. (Master’s thesis).

Appendix

COLLECTION OF DATA AT EACH SITE

Site	Bankfull Width (m)	Channel Width (m)	Channel Depth at Bankfull (m)	Wetted Perimeter (m)	Hydraulic Radius (m)	Slope	Average Bank Height (m)	S.D. Bank Height (m)	Bulk Density (g/cm^3)	S.D. Bulk Density (g/cm^3)
1	22.47	11.11	2.75	23.97	1.87	0.0037	2.22	0.36	1.23	0.02
2	36.03	18.57	1.92	34.85	1.34	0.0008	1.74	0.31	1.28	0.02
3	15.19	10.18	1.19	15.46	0.95	0.0039	1.14	0.19	1.37	0.04
4	21.03	12.08	1.50	21.71	1.16	0.0017	1.50	0.17	1.32	0.02
5	21.06	10.19	2.16	22.31	1.45	0.0029	2.70	0.56	1.43	0.03
6	26.49	21.92	1.78	27.83	1.49	0.0045	1.88	0.16	1.02	0.01
8	14.71	8.69	1.70	15.61	1.26	0.0031	1.58	0.22	1.25	0.01
9	14.57	9.82	1.80	15.98	1.43	0.0024	1.40	0.36	1.33	0.04
10us	9.90	6.00	0.77	10.26	0.58	0.0059	1.12	0.15	1.46	0.00
10mid	9.90	6.00	0.77	10.26	0.58	0.0059	0.94	0.10	1.46	0.00
10ds	9.90	6.00	0.77	10.26	0.58	0.0059	0.94	0.15	1.46	0.00
11us	12.75	5.00	1.15	13.52	0.69	0.0056	0.97	0.10	1.33	0.06
11mid	12.75	5.00	1.15	13.52	0.69	0.0056	1.36	0.49	1.33	0.06
11ds	12.75	5.00	1.15	13.52	0.69	0.0056	0.95	0.23	1.33	0.06
12	30.43	12.41	1.76	31.53	1.28	0.0046	2.47	0.51	1.48	0.03
14	22.45	10.00	1.90	23.34	1.43	0.0067	1.34	0.32	1.36	0.04
16	3.80	0.60	0.54	4.25	0.19	0.0096	0.59	0.10	1.21	0.03

Site	Erosion rate (cm/yr)	Bank Length (m)	Erosion Rate (m^2/yr)	Erosion Rate (kg/yr)	S.D. Erosion Rate (kg/yr)	Percent trees by area (%)	Percent large trees by area (%)	Near-Bank Velocity (m/s)	Bank Strength (kPa)	S.D. Bank Strength (kPa)
1	7.0	97.0	6.83	18673	13778	0.58	0.32	2.79	25.5	7.9
2	36.1	203.4	73.38	163705	29415	0.22	0.14	1.10	28.7	9.2
3	20.1	70.3	14.13	22030	3677	0.17	0.05	2.33	27.0	7.7
4	6.7	104.6	6.99	13871	10705	0.39	0.23	1.30	22.9	8.3
5	13.0	154.0	20.02	77366	16173	0.13	0.07	2.80	43.5	21.4
6	5.5	39.1	2.17	4149	3233	0.72	0.67	4.18	23.2	13.2
8	19.0	43.7	8.31	16371	2288	0.09	0.00	2.05	26.5	13.3
9	8.9	62.0	5.54	10325	9781	0.66	0.58	2.72	27.9	3.8
10us	9.9	45.3	4.47	7311	1004	0.00	0.00	2.16	29.9	4.4
10mid	12.1	32.8	3.96	5443	596	0.00	0.00	1.40	29.9	4.4
10ds	15.3	31.3	4.78	6585	1061	0.00	0.00	2.36	29.9	4.4
11us	2.2	30.0	0.67	856	99	0.69	0.26	1.07	21.5	6.6
11mid	1.4	48.3	0.68	1226	444	0.33	0.27	2.25	21.5	6.6
11ds	4.2	36.1	1.53	1929	475	1.38	1.26	1.48	21.5	6.6
12	9.7	82.8	8.01	29284	24506	1.79	1.56	2.11	49.0	14.4
14	12.5	86.0	10.72	19505	16714	1.16	0.92	3.52	32.3	16.9
16	27.8	17.2	4.78	3420	607	0.00	0.00	1.69	31.8	9.7